

**THE IMPORTANCE OF ELEMENTAL STACKING ORDER AND LAYER
THICKNESS IN CONTROLLING THE FORMATION KINETICS
OF COPPER INDIUM DISELENIDE**

by

JOHN O. THOMPSON

A DISSERTATION

**Presented to the Department of Chemistry
and the Graduate School of the University of Oregon
in partial fulfillment of the requirements
for the degree of
Doctor of Philosophy**

December 2007

“The Importance of Elemental Stacking Order and Layer Thickness in Controlling the Formation Kinetics of Copper Indium Diselenide,” a dissertation prepared by John O. Thompson in partial fulfillment of the requirements for the Doctor of Philosophy degree in the Department of Chemistry. This dissertation has been approved and accepted by:

Dr. James Hutchison, Chair of the Examining Committee

11/26/2007
Date

Committee in Charge: **Dr. James Hutchison, Chair**
 Dr. David Johnson
 Dr. Catherine Page
 Dr. Mark Lonergan
 Dr. David Cohen

Accepted by:

Dean of the Graduate School

© 2007 John O. Thompson

An Abstract of the Dissertation of

John O. Thompson for the degree of Doctor of Philosophy
in the Department of Chemistry to be taken December 2007

Title: THE IMPORTANCE OF ELEMENTAL STACKING ORDER AND LAYER
THICKNESS IN CONTROLLING THE FORMATION KINETICS OF COPPER
INDIUM DISELENIDE

Approved: _____
Dr. David C. Johnson

This dissertation describes the deposition and characterization of an amorphous thin film with a composition near that of CuInSe_2 (CIS). The creation of an amorphous intermediate leads to a crystalline film at low annealing temperatures. Thin films were deposited from elemental sources in a custom built high vacuum chamber.

Copper-selenium and indium-selenium binary layered samples were investigated to identify interfacial reactions that would form undesired binary intermediate compounds resulting in the need for high temperature annealing. Although the indium-selenium system did not form interfacial compounds on deposit, indium crystallized when the indium layer thickness exceeded 15 angstroms, disrupting the continuity of the elemental layers. Copper-selenium elemental layers with a repeat thickness of over 30 angstroms or compositions with less than 63% selenium formed CuSe on deposit.

Several deposition schemes were investigated to identify the proper deposition pattern and thicknesses to form the CIS amorphous film. Simple co-deposition resulted in the nucleation of CIS. A simple stacking of the three elements in the order Se-In-Cu at a repeat thickness of 60 angstroms resulted in the nucleation of CuSe and sometimes CIS. The CIS most likely formed due to the disruption of the elemental layers by the growth of the CuSe. Reduction of the repeat thickness to 20 angstroms eliminated the nucleation of CuSe, as predicted by the study of the binary Cu-Se layered samples, but resulted in the nucleation of CIS, similar to the co-deposited samples.

To eliminate both the thick Cu-Se region, and prevent the intermixing of all three elements, a more complex deposition pattern was initiated. The copper and selenium repeat thicknesses were reduced into a Se-Cu-Se-Cu-Se pattern followed by deposition of the indium layer at a total repeat thickness of 60 angstroms. At a Se:Cu ratio of 2:1 and the small repeat thickness, no Cu-Se phases nucleated. Additionally, the Cu-In interface was eliminated. For this deposition scheme, films with a selenium rich composition relative to CuInSe_2 were generally amorphous. Those that were Cu-In rich always nucleated CIS on deposit. Annealing of all samples produced crystalline CIS.

CURRICULUM VITAE

NAME OF AUTHOR: John O. Thompson

PLACE OF BIRTH: Roseburg, Oregon

DATE OF BIRTH: July 11, 1962

GRADUATE AND UNDERGRADUATE SCHOOLS ATTENDED:

University of Oregon, Eugene, Oregon
Southern Oregon State College, Ashland, Oregon
Umpqua Community College, Roseburg, Oregon

DEGREES AWARDED:

Doctor of Philosophy in Chemistry, 2007, University of Oregon
Bachelor of Science in Chemistry, 2000, Southern Oregon State College

AREAS OF SPECIAL INTEREST:

Materials Science
Solid State Chemistry

PROFESSIONAL EXPERIENCE:

Research Engineer, Hewlett Packard Company, Corvallis Oregon, January 2005-
present

Research Assistant, Department of Chemistry, University of Oregon, Eugene, OR
September 1999-December 2004

Project Scientist, Umpqua Research Company, Myrtle Creek, OR September
1990-June 1999

Nuclear Reactor Operator, United States Navy, September 1986-June 1990

GRANTS, AWARDS AND HONORS:

National Science Foundation: Integrative Graduate Education and Research Traineeship (IGERT) September 2001-Sept 2004

PUBLICATIONS:

John O. Thompson and David C. Johnson, "Synthesis and Characterization of CuInSe_2 , CuGaSe_2 , and Graded Compositions from Modulated Elemental Reactants", *Proceedings of the Electrochemical Society*, 2001, 324-332.

James R. Akse, John O. Thompson, Richard L. Sauer, James E. Atwater, "Reagentless Flow Injection Determination of Ammonia and Urea Using Membrane Separation and Solid Phase Basification", *Microchemical Journal*, 1998, 59, 372-382.

James Atwater, James Akse, John Rodarte, John Thompson, Tsai-Chen Wang, J. Hurley, "Silicon Carbide Coated Granular Activated Carbon: A Robust Support for Low Temperature Aqueous Phase Oxidation Catalysts", *Carbon*, 1997, 35, 1678-1679.

James R. Akse, James E. Atwater, Jeffrey A. McKinnis, John O. Thompson, "Low Temperature Aqueous Phase Catalytic Oxidation of Phenol", *Chemosphere*, 1997, 34, 203-212.

James R. Akse, James E. Atwater, John O. Thompson, "Aqueous Phase Heterogeneous Catalytic Oxidation of Trichloroethylene", *Applied Catalysis B*, 1996, 11, L11-L18.

PATENTS:

Richard L. Sauer, James R. Akse, John O. Thompson, James E. Atwater, Ammonia Monitor, Application US 97-903279.

ACKNOWLEDGMENTS

An individual's graduate program does not exist in a bubble. All who interact with a graduate student leaves their mark. Fellow graduate students share in creating, maintaining, and using tools and equipment necessary for performing the day to day research. Knowledge and ideas are both generated and passed between undergraduates, graduates, professors, and staff.

A university department is not an island. A successful department reaches out to other departments and integrates capabilities and creates collaboration. The successful university does not build walls of academic grandeur, but bridges to industry, so that each may grow in their own way. I can only say that my lab mates, the Chemistry Department, and the University of Oregon got it right.

I would consider myself fortunate to have found the Johnson Lab and the University of Oregon, had it been luck. It was not. It was quite planned and deliberate. I know a winning team when I see one. For this aspect of my graduate program I will take full credit. For everything else I wish to thank everyone who has helped me along the way. Each of you, in your own way has made this journey possible.

To Wilbur and Louise

TABLE OF CONTENTS

Chapter	Page
I. INTRODUCTION	1
Synthesis from Amorphous Precursors	1
How a Solar Cell Works	4
Solar Cell Efficiency	6
Fill Factor	6
The Chalcopyrite Crystal Structure	7
Grain Boundaries	9
Front Interface	9
Back Interface	10
Sodium	11
Alloying with Copper Gallium Diselenide	12
Modern Synthesis Technique	14
Previous Stacked Elemental Layer Techniques	14
Low Temperature Deposition	15
Advantages of the Multilayer Process	16
Summary	17
 II. EXPERIMENTAL	 18
Deposition Chamber	18
Composition	20
Differential Scanning Calorimetry	23
X-ray Diffraction	24
 III. NUCLEATION AND GROWTH OF SELENIUM RICH COPPER SELENIDES FROM AMORPHOUS INTERMEDIATES	 25
Introduction	25
Experimental	28
Differential Scanning Calorimetry of Co-Deposited Copper-Selenium	28
The 50% to 60% Selenium Composition Range	31
The 67% to 81% Selenium Composition Range	32
The 62% to 66% Selenium Composition Range	38
Summary	42

IV. THE EFFECT OF ELEMENTAL STACKING ORDER AND LAYER THICKNESS IN CONTROLLING THE FORMATION KINETICS OF COPPER INDIUM DISELENIDE	44
Introduction.....	44
Experimental.....	46
Indium Selenium Layers.....	47
Copper Selenium Layers.....	50
Copper-Indium-Selenium Layers.....	56
Co-Deposited Selenium-Indium-Copper	59
60 Angstrom Repeat Layered Selenium-Indium-Copper Films	60
20 Angstrom Repeat Layered Selenium-Indium-Copper Films	61
60 Angstrom Repeat Layered Se-Cu-Se-Cu-Se-In Films.....	62
Summary	67
V. THE EFFECT OF SODIUM AND SUBSTITUTION OF GALLIUM ON THE NUCLEATION OF THE CHALCOPYRITE STRUCTURE	69
Introduction.....	69
The Addition of Sodium	69
The Copper Gallium Diselenide Ternary System.....	73
A Comparison of Annealed CIS and CGS Samples	75
Summary	76
VI. SUMMARY AND CONCLUSIONS	78
REFERENCES	81

LIST OF FIGURES

Figure	Page
1.1. Simplified diagram of a <i>p-n</i> junction solar cell	5
1.2. Sample graph for fill factor.	7
1.3. A schematic representation of the copper (indium, gallium) diselenide chalcopyrite structure.	8
2.1. TGOX vs. microprobe composition data for a series of co-deposited copper-selenium samples.....	23
3.1. Reproduction of the copper-selenium binary phase diagram for compositions between 30 and 100% selenium.	27
3.2. DSC scans of co-deposited Cu-Se samples with compositions between 50 and 85 percent selenium performed at a heating rate of 4 °C/min.	29
3.3. XRD data for a sample containing 51% selenium annealed to various temperatures in a DSC at a rate of 4 °C/min.....	32
3.4. XRD data for a sample containing 68% selenium annealed to various temperatures in a DSC.....	33
3.5. DSC scans for 67% selenium samples at heating rates of 4 °C/min. and 10 °C/min.....	35
3.6. XRD patterns of 67% selenium samples heated at 4 °C/min. and 10 °C/min.....	36
3.7. XRD data for a sample containing 79% selenium annealed to various temperatures in a DSC at a rate of 4 °C/min. unless otherwise indicated. ...	37
3.8. XRD data for a sample containing 64% selenium annealed to various temperatures in a DSC at a rate of 4 °C/min.....	38
3.9. XRD data for a sample containing 66% selenium annealed to various temperatures in a DSC at a rate of 4 °C/min.....	39

Figure	Page
3.10. Kissinger plot used to derive the activation energy for nucleation of cubic CuSe ₂	41
3.11. XRD patterns for a 64% selenium sample soon after deposition and 44 months later.	42
4.1. X-ray reflectivity scans of indium selenium layered thin films.	48
4.2. Total repeat thickness (circles) and composition (squares) vs. indium layer thickness.	49
4.3. Indium crystallization at layer thicknesses above 15 angstroms.	50
4.4. XRR data for Cu-Se layered films at compositions between 57 and 69% selenium at three different repeat thicknesses.	52
4.5. XRD patterns for layered copper-selenium samples.	54
4.6. Summary of XRD results for copper-selenium layered and co-deposited films.	55
4.7. Schematic representations of the three repeat layering schemes used to investigate the effect of layer repeat thickness and order.	56
4.8. Summary of deposition results indicating the stacking order/thickness and composition resulting in as-deposited nucleated and amorphous films.	58
4.9. XRD patterns for copper, indium, and selenium co-deposited onto quartz to a depth of approximately 3000 angstroms.	59
4.10. XRD scans for Se:In:Cu films with a 60 angstrom repeat thickness.	60
4.11. XRD patterns for thin film samples deposited in the order Se:In:Cu with a 20 angstrom repeat thickness.	62
4.12. XRD patterns for the as-deposited Se-Cu-Se-Cu-Se-In films deposited at a repeat thickness of 60 angstroms and 5000 angstroms total thickness.	63
4.13. XRR patterns for some amorphous Se-Cu-Se-Cu-Se-In thin films.	64

Figure	Page
4.14. XRD patterns for an amorphous CIS film annealed to 500 °C.....	66
4.15. The increase in crystallite size for an amorphous CIS sample annealed at 100 °C increments to 500 °C.....	67
5.1. Comparison of sodium and non-sodium containing Se-Cu-Se-Cu-Se-In samples for crystallinity on deposit.....	71
5.2. A Comparison of sodium and non-sodium containing Se-Cu-Se-Cu-Se-In samples for crystal size after annealing to 500 °C in nitrogen.	72
5.3. XRD patterns for as-deposited Se-Ga-Cu layered films.	75
5.4. Summary of crystallite sizes for annealed films of CIS/CGS.	76

LIST OF TABLES

Table	Page
5.1. Deposition consistency for five Se-Ga-Cu samples	74

CHAPTER I

INTRODUCTION

Synthesis from Amorphous Precursors

The synthesis of new solid state compounds is difficult. To make a new metastable compound, you first need to avoid forming all of the thermodynamically stable compounds in the phase space being explored. Control of kinetics during the formation of new phases is crucial in the synthesis of new compounds. Alternatively, the uncontrolled formation of phases is quite simple. In just one solid state combinatorial experiment involving materials with compositionally variable phases, almost an infinite number of different compositions can be produced, most of which will produce a mixture of phases. Analysis and characterization of these phases to find the new ones or to find samples with the desired properties becomes the rate limiting step to the discovery of new, usable materials. Although the combinatorial approach has shown its worth, especially when combined with a kinetic approach rather than the traditional heat and beat synthesis approach, a rational approach targeting specific compounds of interest significantly reduces analysis time.

Generally speaking, most inorganic solids are produced from a high temperature reaction. If a homogeneous melt is required, a sufficiently high temperature must be achieved to melt not only the initial components, but also any intermediate compounds formed at the interface of the precursor solids and those formed by the precursors'

interface with the liquid phase. Controlled cooling and annealing of these melts are used to impart properties in the solid that deviate from the thermodynamically stable phases producing a 'metastable' product.

When one looks at the surface of the Earth, one realizes that 'metastability' is the rule and not the exception. Stability relies heavily on how one defines the system. Steel, slowly cooled from a melt, is thermodynamically stable, but when placed in an oxygen containing environment, it is not stable relative to its oxide. In a similar fashion, an isolated crystalline layer of a pure element is considered to be thermodynamically stable. When placed in intimate contact with another element or compound capable of inter-diffusion or phase formation, the system becomes metastable. One method of creating new compounds or stable compounds at temperatures below the melting point is to take advantage of the metastability of stacked thin elemental layers. By judicious control of elemental layer thickness, layer order, and thermal annealing conditions including time, temperature, atmosphere, and pressure, metastable precursor materials and stable phases can be produced at low temperature.

In a simple binary system, there is only one type of interface between the two elemental layers, and of course the front and back surfaces. For these systems, a 'critical thickness' has been defined as the transition point between complete inter-diffusion before nucleation, and phase formation at the interface before diffusion is complete. Either situation may be desirable depending on the targeted phases(s) and structure. Nucleation at an interface can result in a preferred alignment of the growing

crystallites. Complete diffusion before nucleation can be utilized to create a metastable amorphous intermediate that is further processed to form a crystalline phase. Elemental layer interaction becomes more complex when three elements are deposited as thin layers. There are now up to three elemental interfaces involved. Ternary layering has previously been used to form superlattices of two different binary phases with the common element to both phases separating the other two elements.^{1,2,3} If one wishes to form a single phase from an amorphous precursor consisting of the three elements, then the layer thickness is limited to prevent nucleation of binary compounds before diffusion is complete. The question becomes, why not just co-deposit the three elements to form the amorphous precursor? Indeed this process will work, assuming that a binary or ternary phase does not nucleate under ambient deposition conditions.

The desire for an amorphous precursor for the copper indium diselenide system has led to the investigation of how the order and thickness of the elemental layers affect nucleation and growth of copper indium diselenide. In addition, the effects of the addition of sodium on nucleation and growth of the CIS phase and the substitution of gallium for indium was investigated. In this dissertation, I will present data characterizing the elemental layering, nucleation, and/or crystal growth of binary copper-selenium, binary indium selenium, ternary copper indium diselenide (with and without sodium), and copper gallium diselenide thin film layered systems.

The motivation for this work has been to produce an amorphous thin film layer stack from which CIS can be formed on heating. Nucleation of CIS during deposition would necessitate a high temperature anneal to drive crystal growth via an Ostwald

ripening process. The reduction of the necessary annealing temperature would enable the use of inexpensive substrates that are unable to withstand high temperatures. Additionally, low temperature annealing would open the door to the design of solar cell absorber layers with controlled graded band gaps via the adjustment of the Ga/(Ga+In) ratio. To better understand how the control of thermal history may lead to improvements in solar cell performance, a brief review of CIGS solar cell technology is included.

How a Solar Cell Works

A brief review of CIS type solar cells is in order to ground the reader with the technology and challenges with the CIGS material system and its interfaces with other solar cell materials. For electronic materials such as CIS, formation of the desired phase is only the first step in optimizing the material. The electronic properties, compared to the structural properties, are always more sensitive to the process used to make the desired phase. In addition, the formation of the electrical interface with other phases is often crucial to achieve the desired device characteristics.

Figure 1.1 shows a simplified diagram of a solar cell. In its most simplified form, a solar cell is composed of a semiconductor doped as n-type on one side and p-type on the other, effectively a large flat bipolar diode. A conductive material on each surface is used to collect charge carriers.

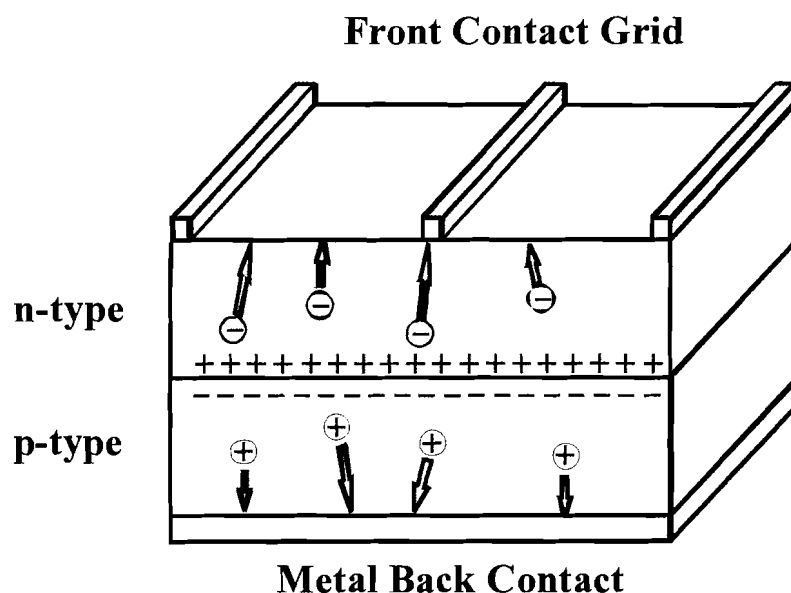


Figure 1.1 Simplified diagram of a p - n junction solar cell.

A solar cell works on the principle of charge carrier excitation in the presence of a static electric field. When an n -type and a p -type semiconductor are in intimate contact, electrons in the n type material migrate to the p type material until the electrostatic field produced by the charge imbalance counteracts the chemical potential. The resulting transfer of charge carriers produces a permanent electric field across the junction. Photons with energies greater than the band gap of the absorber layer may interact with a valence band electron and promote it to the conduction band leaving a hole. The static electric potential causes the electrons to migrate in the direction of the n type material and the holes to migrate in the direction of the p type material. The electrons and holes then travel through the conductive surface contacts and recombine in the external electrical load resulting in a current loop.

Solar Cell Efficiency

Cell efficiency is a measure of the amount of usable electric energy that a solar cell produces relative to the amount of light striking the surface of the solar cell.

The efficiency of a solar cell depends on both the efficient absorption of photons to generate carriers and the transport of those carriers. Recombination or charge trapping, where an electron and hole recombine in either the absorber layer or the interfaces reduces the efficiency of a solar cell. The usable energy of the charge carriers is determined by the band gap of the absorber layer which establishes the maximum voltage that can be produced by the cell. The current is determined by the number of photons that promote an electron from the valence band to the conduction band resulting in free charge carriers which may reach the external circuit. Since the solar spectrum is fixed, a trade off exists between voltage and current. A wide band gap material will utilize less of the solar spectrum but retain more of the energy from each created charge carrier pair. A narrow band gap material can use more of the solar spectrum but produce less energy per charge carrier pair.

Fill Factor

The fill factor is a measure of a solar cells operational efficiency relative to its maximum current and voltage. The open circuit voltage (V_{oc}) is the physical measurement of the maximum voltage a solar cell will produce with no current flow, thereby eliminating voltage drops through the cell. The maximum voltage that a solar cell can produce is limited by the photon absorber's band gap. The short circuit current

(J_{sc}) is the maximum current that a solar cell can produce under no electrical load. The maximum current is limited by the number of photons striking the surface with enough energy to produce an electron hole pair. Fill factor, graphically represented in figure 1.2, is a comparison between the power produced by a solar cell under a standard load and the theoretical maximum of the product of J_{sc} and V_{oc} . Fill factor is commonly used to compare solar cells and identify inefficiencies in solar cells.

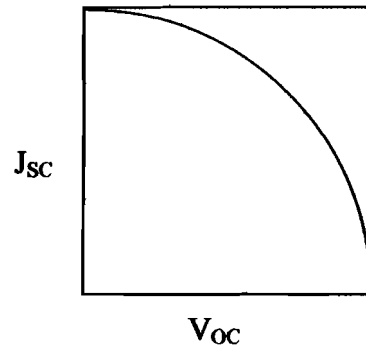


Figure 1.2. Sample graph for fill factor. A fill factor of 100% would be represented by the rectangle. A real cell is represented by a curve similar to the one pictured.

The Chalcopyrite Crystal Structure

Copper indium diselenide (CIS) is a commonly used absorber layer in solar cells. CIS is a member of the chalcopyrite mineral family with a general composition of $I_1III_1VI_2$. The crystal structure is tetragonal (figure 1.3), space group $I4(\bar{2})2d$ with lattice parameters of $a, b=5.78$ angstroms and the c parameter being about twice that of the a, b parameters at 11.6 angstroms.⁴ Each copper and indium is tetrahedrally coordinated with four selenium atoms as closest neighbors. Each selenium atom has two copper and two indium atoms as closest neighbors. A series of ordered vacancy

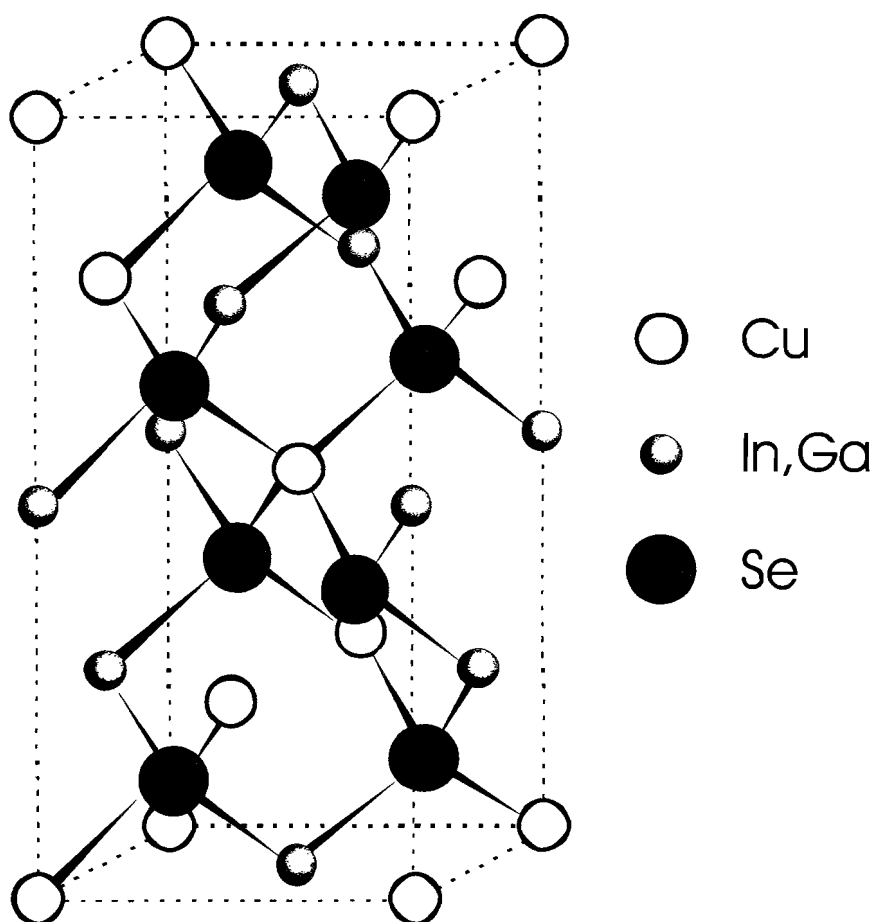


Figure 1.3. A schematic representation of the copper (indium, gallium) diselenide chalcopyrite structure.

compounds exist (CuIn_3Se_5 , CuIn_5Se_8 , etc.) produced by the substitution of an indium on a copper site (In_{Cu}) and the creation of two copper vacancies (V_{Cu}) necessary for charge neutrality. The ordered vacancy compounds exist as stable structures due to the low formation energy of the In_{Cu} substitution and copper vacancies.⁵ Copper indium diselenide has a large compositional range in the indium rich, copper poor portion of the ternary phase space ($\text{In}_{1+x}\text{Cu}_{1-x}\text{Se}_2$). There is very little solubility for excess copper in

the CIS structure, with excess copper forming copper selenide impurities.⁶

Composition determines if the material is *n* type or *p* type. CIS can be *n* type with a Cu/In ratio of less than 0.73. The material used to make solar cells is *p* type with a Cu/In ratio between 0.73 and 1.0.⁷

Grain Boundaries

Grain boundaries have been identified as major sites for carrier recombination in most polycrystalline electronic materials. CIS is unique in this regard because polycrystalline CIS has similar electrical properties to single crystalline CIS. Optimized CIS solar cells have been shown to be copper-poor at the surface. The composition of the surfaces tends to indicate that a layer of the ordered vacancy compound CuIn_3Se_5 forms at the surfaces of the CIS grains. The creation of this layer can be enhanced by indium rich deposition conditions in the final stage of absorber layer deposition. This copper poor layer is intrinsically n-type and forms a repulsion field for the electrons, effectively shielding the surface and reducing recombination. Calculations performed by Rockett, has shown that defects such as $\text{V}_{\text{Cu}}\text{-In-V}_{\text{Cu}}$ sets form super clusters whose surfaces are charged. The surface charge on these clusters of defects repels charges and reduces recombination losses by the defects.⁸

Front Interface

The front interface of the highest efficiency CIGS based solar cell is composed of a cadmium sulfide layer deposited via chemical bath deposition, a highly resistive

zinc oxide layer and an aluminum doped conductive zinc oxide layer, both sputter deposited. The final layer is a metallic grid that collects and delivers the charge carriers to the external surface. For the purposes of this project, I will focus my review on the CIGS/CdS interface and how it affects optimization of the CIGS layer. The CIGS/CdS interface was first thought to be a heterojunction with the p/n interface at the material interface. There is now compelling evidence that the actual p/n junction is buried in the CIGS layer. There is a significant advantage to a buried junction in that recombination at the p/n junction is reduced and one can now focus on optimizing the material interface.⁹

Back Interface

For many years now, molybdenum has been the overwhelming choice for the back conductive charge collector and interface with the CIS absorber layer. During growth of the CIS layer at elevated temperatures, a randomly oriented MoSe₂ layer forms between the CIS and molybdenum metal, eliminating the Schottky barrier formed by the CIS/Mo junction and replacing it with an ohmic electrical interface. Simply growing a MoSe₂ layer on the molybdenum before CIS deposition produced highly oriented MoSe₂ with its c-axis perpendicular to the Mo surface. Since MoSe₂ is a layered van der Waals gap type structure, this orientation often results in delamination of the MoSe₂ from the Mo surface.^{10, 11, 12}

Sodium

Historically, sodium was inadvertently added to the CIS layer during thermal deposition through diffusion from soda lime glass substrates. It was observed that samples grown on molybdenum coated soda lime glass produced higher efficiency solar cells compared to those grown on molybdenum coated borosilicate glass. Initially, the improvement was believed to be due to compatible thermal expansion coefficients between the soda lime glass and the CIS layer. Later, it was determined that sodium was diffusing through the molybdenum layer into the CIS material. A lot of speculation surrounded this new discovery.¹³

It has been determined that the major effects of the presence of sodium are an increased hole density increasing film conductivity, and suppression of the formation of the CIS ordered vacancy compounds. Theoretical calculations performed by Wei, has shown that the effects that sodium has on the CIS structure depends on the amount of sodium available during crystal growth. The major effect of trace amounts of sodium is the destabilization of In_{Cu} defects with the indium being replaced by sodium. The loss of the In_{Cu} substitution defects eliminates the population of the $(\text{V}_{\text{Cu}}^- + \text{In}_{\text{Cu}}^{2+} + \text{V}_{\text{Cu}}^-)$ clusters and destabilizes the ordered vacancy compound (OVC) structures. Further addition of sodium results in nucleation and growth of a secondary phase composed of NaInSe_2 .¹⁴

The presence of sodium has shown the unexpected side effect of reducing gallium and indium diffusion in CIGS as it is being deposited. Lundberg and coworkers have shown that with sodium present, Ga-In diffusion is suppressed in both copper rich

and copper poor samples. The diffusion is believed to be higher in sodium free films due to increased concentration of metal vacancies. Additionally, they observed that the diffusion pathway is similar through the grains as through the grain boundaries.¹⁵ The control of metal diffusion will play a vital part in creating CIGS layers with a graded composition.

Alloying with Copper Gallium Diselenide

The alloying of CuGaSe₂ (CGS) with CuInSe₂ to form CIGS has been used to improve the properties of the absorber layer and its interfaces with the other cell layers. The crystal structure of CGS is the same as the CIS chalcopyrite structure with larger lattice parameters with the a,b parameters being 5.5963 angstroms and the c parameter being 11.0036.⁶ By far, the most important reason for alloying CGS with CIS is to increase the band gap of the material. The optimal band gap of the absorber layer for our solar spectrum is 1.4 eV, maximizing cell power.

The increase in band gap with CGS alloying is nearly linear and follows the equation:

$$E_g(x) = (1-x)E_g(\text{CIS}) + xE_g(\text{CGS}) - bx(1-x)$$

where $E_g(x)$ is the band gap at a gallium to indium atomic ratio of $x = \text{Ga}/(\text{Ga}+\text{In})$ and b is the bowing coefficient equal to about 0.15-0.24 eV for this material system.¹⁶ Theoretical band offset studies of the CIS/CGS interface using a first-principles band

structure method, has determined that the offset is predominately at the conduction band level and only a small offset exists at the valence band level.¹⁷

Alloying with CGS also reduces the stability of the ordered vacancy compounds relative to the 1:1:2 CIS structure.¹⁷ The destabilization of the OVC phases also results in defect cluster destabilization and a loss of the OVC phases at the surface of the grain boundaries which normally shield the carriers from recombination centers at the surface. Calculations performed by Zhang and others identified the band gap of the CIS OVC's present in CIS structures as being between 1.17 and 1.28 eV.⁵ For CIS with a band gap of 1.0 eV, the OVC structural defects are electrically benign due to their large band gaps. The increase in band gap of CIGS with increasing gallium content, results in the OVC structures now being sites for charge recombination. For these reasons, the gallium fraction is usually kept at or below about 0.3 Ga/(Ga+In), even though this band gap of 1.2 eV is not ideal for the solar spectrum.

The best cell efficiency will be realized utilizing a graded Ga/(In+Ga) composition. The primary objective is to simultaneously optimize current, voltage, and fill factor. The V_{oc} is primarily determined by the highest band gap in the space charge region of the absorber layer; however a high band gap reduces the percentage of usable photons that will generate carriers. This inefficiency can be partially overcome by reducing the Ga/(In+Ga) outside the space charge region so the lower energy photons can be absorbed.^{18, 19}

Modern Synthesis Technique

The current technique producing the most efficient CIGS based solar cells uses a three stage process developed at NREL. In the first stage, indium, gallium, and selenium are co-deposited onto a molybdenum coated soda-lime glass substrate heated to a temperature between 250 and 300 °C. The composition of the absorber layer at this stage is $(\text{In}_x\text{Ga}_{1-x})_2\text{Se}_3$. It has been shown that this In,Ga rich layer forms a thicker MoSe_2 layer at the interface. The precursor layer is then exposed to a copper selenium flux at a substrate temperature of 540 °C until the material is slightly Cu rich relative to the In and Ga. The copper rich composition will enhance grain growth through the formation of a molten Cu-Se growth flux layer on the surface of the grains. In the final stage, additional indium and selenium are added to adjust the composition back to the desired In, Ga rich stoichiometry.²⁰ Adjustments on the three stage growth process later resulted in a record breaking CIGS solar cell with an efficiency of 18.8 percent.²¹ The current three stage synthesis technique limits the ability to grade the gallium composition. Precise gallium grading is more compatible with evaporation techniques requiring low substrate temperatures.²²

Previous Stacked Elemental Layer Techniques

Copper indium diselenide has previously been made from stacked elemental processes.^{23, 24, 25} Knowles, et al annealed elemental stacks of copper, indium, and selenium layers with a total repeat thickness of 1560 angstroms. Annealing at 500 °C for a half hour produced crystalline CIS with a 112 preferred orientation.²³ Karg and

coworkers found that rapid thermal annealing of stacked elemental layers, as compared to vacuum oven annealing, produced a solar cell with much higher efficiencies, over 10% as compared to less than 3%. They attributed the improvement to the rapid heating rate minimizing the production of binary intermediates and dewetting problems experienced in conventional annealing methods.²⁴ Generally, the processes included thermal deposition of relatively thick layered elemental stacks with individual layers on the order of several hundred angstroms thick followed by laser or thermal annealing. Due to the thickness of the layers, high temperatures at or above 500 °C were necessary to ensure complete mixing and crystallization. Many of these techniques did produce the chalcopyrite phase of CIS but never produced cells with record efficiencies. The high temperatures necessary to fully react thick elemental layers restricts the selection of a substrate to one that is stable under these conditions.

Low Temperature Deposition

The desire to utilize substrates which are structurally sensitive to high temperatures, such as polyimide films, has led to a search for low temperature processing conditions that would result in device quality CIGS materials. Nishiwaki and coworkers used the first two stages of the standard three stage process to grow CIGS films on Mo-coated soda lime glass substrates at temperatures from 350 to 500 °C. They found that the sample grown at 350 °C contained a Cu/Se gradient with less

copper at the back of the cell but no gradient in the samples grown at higher temperatures. A CIGS cell manufactured from the film deposited at 350 °C showed an efficiency of 12.4%.²⁶

Advantages of the Multilayer Process

To use low cost flexible substrates and to develop the capability of multi zone grading of the indium:gallium ratio in the CIGS structure, a synthesis technique that is effective at low temperatures is required. The presence of crystalline material in the deposited layers would necessitate high temperature annealing to convert the film to large CIGS grains. Therefore, an amorphous intermediate that could undergo rapid thermal annealing to form the CIGS material is desirable. The magnitude of this challenge becomes clear when one considers that co-deposited Cu-In-Se will form crystalline CIS on deposit at ambient temperature necessitating a high temperature Ostwald ripening process to grow large CIGS grains. Generally, if the layers are deposited thick enough to prevent inter-diffusion and formation of the CIGS structure, binary compounds will form at the elemental interfaces, necessitating high annealing temperatures to react the crystalline binary compounds with the remaining mass to form the CIGS compound. The ability to form an amorphous thin film precursor, with compositional modulation on a small length scale may allow us to control initial nucleation and grain growth. This control could lead to an annealing process that utilizes low temperatures for crystallization of the CIGS while limiting indium/gallium interdiffusion, and ultimately allow for the use of lower temperature substrates.

Summary

The next four chapters will summarize my work toward the goal of creating an amorphous thin film structure for the synthesis of a CI(G)S layer. Chapter II will describe the unique characteristics of the vacuum deposition chamber used to deposit the elemental layers for this research. Additionally, the instrumental methods used to characterize the composition, layering, and phases of the materials formed will be described. Chapter III will describe the results for co-deposited copper-selenium powder samples characterized by DSC and XRD. Chapter IV will discuss the process by which an amorphous copper-indium-selenium thin layer precursor is formed via control over elemental layer order and thickness. This chapter will also include relevant results for layered copper-selenium and layered indium selenium work that was utilized to create the amorphous CIS precursor.

Chapter V will discuss the deposition, annealing, and characterization of thin film Cu-In-Se samples containing sodium and compare them to films with no sodium. Additionally the deposition, annealing, and characterization of some CGS samples will be described and the results compared to compatible CIS samples.

CHAPTER II

EXPERIMENTAL

Deposition Chamber

The films described in this work were deposited in a custom built high vacuum chamber maintained at a vacuum of 1×10^{-6} Torr or below. The chamber is equipped with four positions for mounting thermal sources. Each thermal source has a quartz crystal monitor mounted above it to quantify the deposition rate. The thermal sources are all directed at the same rotating substrate holder approximately 22 inches above the thermal sources. The cycling of shutters between the thermal sources and substrate determine the deposited layer thicknesses. The substrate is rotated to improve deposition consistency across the six inch substrate mount. Due to the long deposition times of up to seven hours for making thick CIS samples, special procedures were developed to ensure consistent deposition over a long time span.

Copper was deposited from an e-beam gun using a glassy carbon crucible for thermal isolation from the e-beam guns hearth. After several hours of deposition, the as received copper formed an insulating film across the molten slug that blocked the copper flux, producing an erratic deposition rate and resulting in cyclical power surges to the e-beam gun. The presence of the film was eliminated by pre-melting the copper in the chamber and polishing the cooled slug with sand paper followed by an acetone

rinse. This process was repeated until visual observation of the molten copper indicated that no residue remained.

Selenium, sodium, indium, and gallium were all deposited from effusion cells. Gallium cannot be deposited from an e-beam gun for extended periods of time due to the liquefaction of the gallium on the quartz crystal monitors surface resulting in an artificially low reading of deposition rate and thermal run away of the e-beam gun. To circumvent this problem, the gallium was deposited from an Applied Epi SUMO™ cell. This cell is designed to maintain a stable temperature and flux for several hours. The cell was rapidly heated and the deposition rate established before the gallium liquefied on the quartz crystal surface. Deposition was then performed according to shutter cycling time assuming a stable deposition rate. Selenium was also deposited from a SUMO™ cell equipped with a top insert. Although the selenium source was stable, the thickness reading from the crystal monitor was used to cycle the shutter. Sodium was also deposited from a SUMO™ cell. Desired deposition rate was almost impossible to quantify, so the desired deposition rate was determined via compositional analysis of previous samples.

The deposition of indium presented a special problem. Small amounts of selenium vapor, probably re evaporated from surfaces inside the chamber, were depositing onto the indium quartz crystal. The presence of the selenium in the indium produced a non linear effect on deposition rate indication. After several hours of deposition, not only did the deposition rate become inaccurate, but the crystal would often completely fail. To circumvent this problem, a shield was installed around the

path of the indium flux from near the indium source to the crystal monitor surface. Additionally, like the gallium, deposition rate was established and the shutters were cycled by time.

The elemental sources were deposited onto a rotating six inch diameter silicon wafer located approximately 22 inches above the elemental sources. The wafer was coated with polymethylmethacrylate (PMMA), which was later dissolved in acetone to release the deposited material for collection on a filter paper. Additionally, small chips of silicon were attached to the surface of the silicon wafer for use in compositional analysis and to observe layering via X-ray reflectivity. Sometimes, pieces of off-angle cut, polished quartz were also mounted for annealing studies when interference at high XRD angles was to be avoided. The target wafer was not actively heated or cooled during deposition.

Composition

The composition of CIGS samples must be accurately determined to produce usable samples. The CIS phase cannot accommodate excess copper in the structure and will produce Cu_{2-x}Se impurity phases which will result in electrical shorting. The copper to indium ratio will affect whether the material is *n*- or *p*- type and the level of doping. While the loss of excess selenium during annealing will create excessively large grain boundaries and crevice formation, insufficient selenium will result in the formation of binary phases in the sample. A narrow compositional range around the $\text{In}_2\text{Se}_3\text{-Cu}_2\text{Se}$ tie line must be adhered to in order to produce quality samples.

The composition of samples has been determined using two different methods: Electron Probe Microanalysis (microprobe) and, for some copper selenium binary samples, thermal gravimetric oxidation (TGOX). TGOX can be used for binary samples containing selenium and takes advantage of the creation of thermally stable copper or indium oxides and the loss of selenium at high temperatures in air. This method consists of slowly heating a pre-weighed sample in air to a final temperature of 800° C and held for 30 minutes. During this time, the selenium volatilizes out of the sample and indium or copper is oxidized to In_2O_3 or CuO respectively. After oxidation, the sample is reweighed with the sample weight attributed to the metal oxide. In this work, a TA Instruments model 2950 thermogravimetric analyzer was used to oxidize the samples and quantify the mass loss. The primary disadvantage of this method is that only binary samples can be analyzed.

Microprobe data was collected on a Cameca XS 50 electron probe microanalyzer. Microprobe utilizes high energy electrons as the activation source to induce the emission of characteristic x-rays from elements in the sample. The x-rays are formed in a one micron diameter or smaller sphere near the surface of the sample. The x-rays are then detected and quantified by various types of detectors. These signals are further fed into an algorithm which takes into account a calibration curve and shielding of the x-rays by the elements in the sample. Although the microprobe technique can be as accurate as 1%, there are several sources for error which must be considered. The primary concern with respect to thin film samples is the sample thickness. The algorithm used to calculate atomic composition assumes that the sample

is continuous and at least one micron thick, the activation area produced by the high energy electrons. When the sample is too thin, the x-ray flux for some elements will be preferentially affected. This will lead to an inaccurate calculation of composition. Since thin film samples are usually less than a micron thick, the sample pieces are stacked to produce a micron thick sample. Simple stacking may lead to low density of material and erroneous results.

In the later parts of my research, a new thin film modeling technique was used to determine sample composition. This new technique uses the intensities of characteristic x-rays produced at several electron accelerating energies. If the composition of the substrate is known, silicon in this case, the sample can be modeled using the StratagemTM software package. From these intensities, both composition and, to a lesser degree, thickness of the sample can be determined. A comparison between TGOX and microprobe data for a series of co-deposited copper selenium samples is presented in figure 2.1 and shows this to be a viable technique for composition determination.

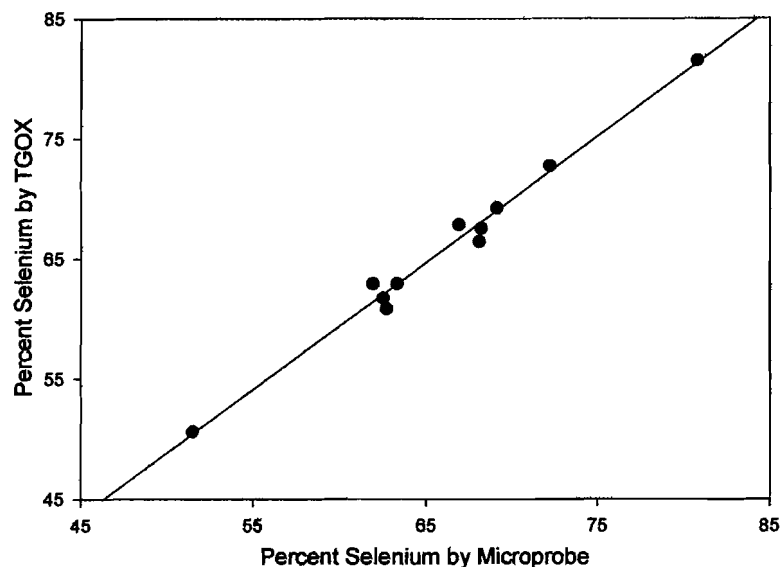


Figure 2.1. TGOX vs. microprobe composition data for a series of co-deposited copper-selenium samples.

Differential Scanning Calorimetry

Differential scanning calorimetry (DSC) is a method of determining the amount of heat evolved or absorbed from a material during a constant temperature change. In this project, the materials were analyzed on a TA Instruments model 2920 modulated DSC. The DSC can be run in either normal or modulated modes. In normal mode, the DSC heats the sample and a reference at a constant rate between two temperatures. The thermal scan can then be repeated as a method of subtracting off the background signal to better define weak peaks. In modulated mode, the sample is heated in stages of a few degrees and then slightly cooled. Reversal of the heat flow on cooling indicates reversibility in the thermal event occurring. Modulated mode is better for identifying weak thermal events. One must also consider that the former mode, when using a

second scan to subtract background interference, is comparing the sample as it is reacting (the first scan) to that of the final product after it is fully annealed (the second scan) while the latter method is comparing the sample to itself at that temperature during the scan.

X-ray Diffraction

Three different X-ray diffractometers were used to collect X-ray Diffraction (XRD) and X-ray Reflectivity (XRR) data on as-deposited and annealed samples. The Scintag XDS 2000 was used to collect XRD and XRR data from powder and substrate supported samples, while the Philips X'Pert MRD and Bruker D8 Discover Diffractometer were used to collect data from supported samples. No distinction will be made between data from the three diffractometers unless special features of the diffractometer were used.

CHAPTER III
NUCLEATION AND GROWTH OF SELENIUM RICH COPPER
SELENIDES FROM AMORPHOUS INTERMEDIATES

Introduction

The synthesis of most molecular compounds occurs in a homogeneous, liquid environment. In this environment, diffusion is rapid and is often aided by agitation of the solution. Most desired organic products are metastable, so both reaction duration and temperature are regulated to maximize the yield of the desired product. Generally speaking, most inorganic solids are produced from a high temperature melt of the component elements. A sufficiently high temperature must be achieved to melt not only the initial components, but also any intermediate compounds formed at the interface of the precursor particles and those formed by the precursors interface with the liquid phase. Controlled cooling and annealing programs are used to impart properties in the solid that deviate from the thermodynamically stable phases.

A co-deposited precursor eliminates undesired intermediate reactions by eliminating particle-particle interfaces. Similar to molecular synthesis, the precursor is initially homogeneous. Unlike molecular synthesis, diffusion is not aided by agitation,

and may be the rate limiting step of a reaction. In this chapter, we will discuss the evolution of copper selenium phases from selenium rich co-deposited samples from thermal sources.

Several binary phases of the copper-selenium system have been thoroughly explored under both ambient conditions and at elevated temperature and pressure.^{1, 2, 3} Copper selenium binary compounds have previously been investigated for their photovoltaic properties.^{4, 5, 6, 7, 8} Additionally, CuSe has been used as a precursor layer for the formation of copper indium diselenide from a selenized stacked elemental layer.^{9, 10, 11} CuSe and orthorhombic CuSe₂ have been identified as impurity phases in copper indium diselenide grown by electrodeposition and vacuum deposition processes.^{12, 13, 14} Binary copper-selenium compounds have been made by several methods including melt techniques,^{1, 2, 3} mechanical alloying,¹⁵ electrodeposition,¹⁶ plasma assisted selenization,¹⁷ and at aqueous-organic interfaces.¹⁸

The use of CuSe and CuSe₂ as precursors in the synthesis of, and their presence as secondary phases in copper indium diselenide prompted this study of the nucleation and growth kinetics of the selenium rich portion of the copper-selenium phase diagram. This chapter examines the evolution of amorphous precursors prepared by co-depositing the elements on a cold substrate. XRD and DSC were used to explore the phase evolution of the samples as a function of annealing rate and temperature. Surprisingly we observed the nucleation and growth of the metastable phase cubic CuSe₂ over a broad composition range at moderate temperatures.

The Cu-Se phase diagram was explored in the 1960's³ and the crystal structures of the phases and phase formation at elevated temperature and pressure in the 70's.^{1, 2} The phase diagram contains three selenium rich compounds as shown in figure 3.1.¹⁹ CuSe has three polymorphs. The form of CuSe stable at room temperature is hexagonal α CuSe. α CuSe undergoes a reversible polymorphic change to orthorhombic β CuSe at 51 °C and then to hexagonal γ CuSe at 120 °C. γ CuSe peritectically disproportionates into β (Cu_{2-x}Se) and a selenium rich liquid phase at 377 °C. The composition of CuSe₂ has two polymorphs. The thermodynamically stable phase is orthorhombic and

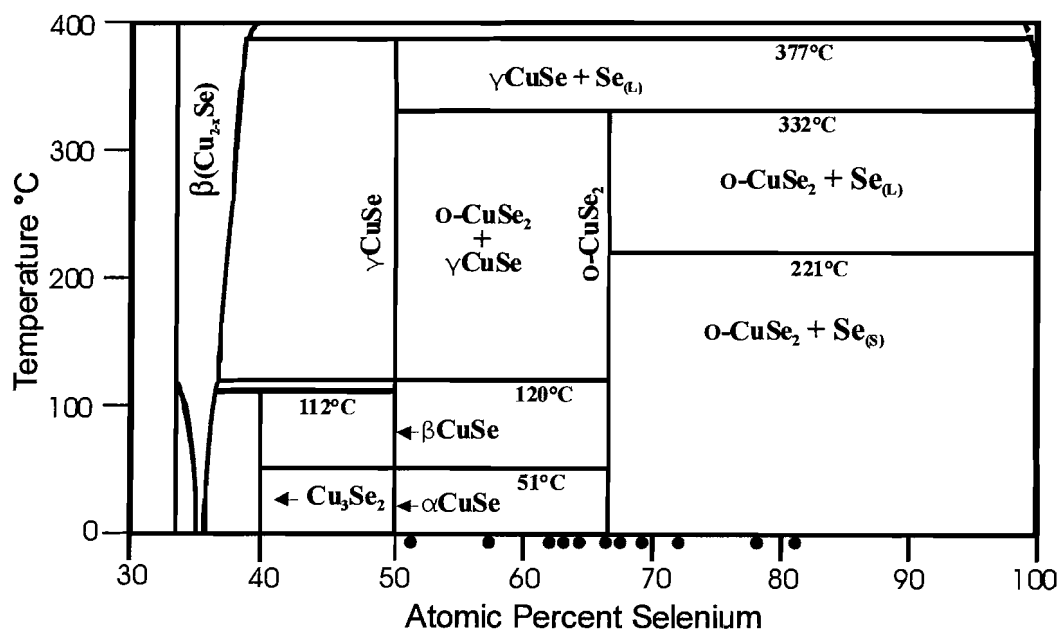


Figure 3.1. Reproduction of the copper-selenium binary phase diagram for compositions between 30 and 100% selenium.¹⁹ The black dots along the selenium percentage axis represent compositions that were investigated.

peritectically disproportionates into CuSe and a selenium rich melt at 332 °C. The orthorhombic phase is grown through slow cooling from a melt.¹ The metastable polymorph is cubic and can be produced by annealing orthorhombic CuSe₂ at 12kbar and 420 °C for 2 hours followed by rapid cooling.¹ Cu₃Se₂ was not observed in the composition range and annealing conditions studied.

Experimental

The co-deposited copper selenium films described in this study were deposited as described in chapter II. The target wafer was coated with polymethylmethacrylate (PMMA), which was later dissolved in acetone to release the deposited material for collection on a filter paper. Additionally, a small chip of silicon was attached to the surface of the silicon wafer for use in compositional analysis by microprobe. The target wafer was not actively heated or cooled during deposition. Duration of the deposition was selected to ensure sufficient quantity of sample for analysis.

Differential Scanning Calorimetry of Co-Deposited Copper-Selenium

Samples were prepared by co-depositing the elements onto a cold substrate varying the ratio of the deposition rates to prepare samples between 50 and 85% selenium. Figure 3.2 contains the DSC scans of these samples performed at a heating rate of 4 °C/min. The atomic percent of selenium in each sample is indicated by where the DSC scan begins on the left Y-axis. The behavior of the samples can be roughly divided into three different groups depending on their concentration. Below 60%

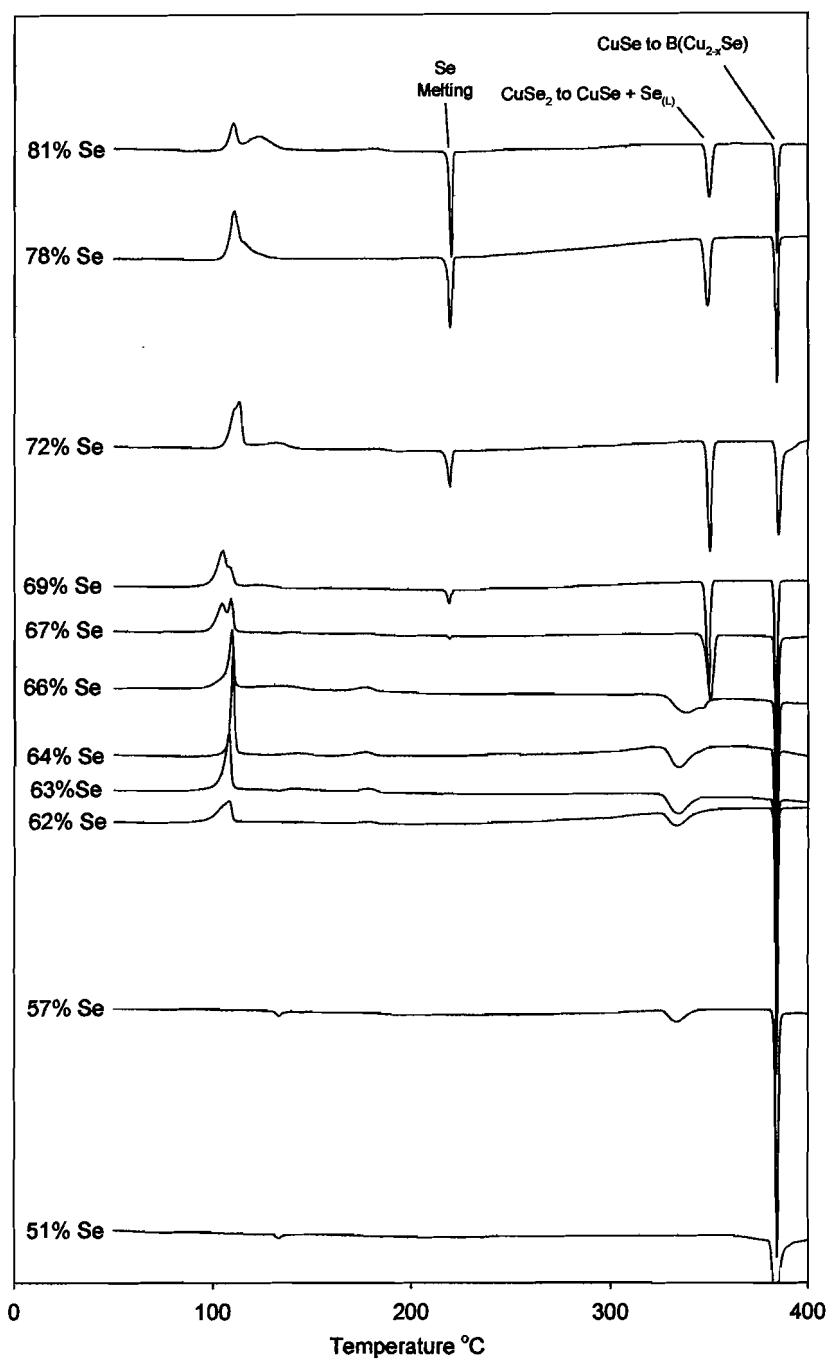


Figure 3.2. DSC scans of co-deposited Cu-Se samples with compositions between 50 and 85 percent selenium performed at a heating rate of 4 °C/min. Exotherms are indicated in the upward direction.

selenium, hexagonal CuSe forms as-deposited. Between 62% and 66% selenium the samples are amorphous as-deposited and have broad exotherms between 330 and 350 °C. Above 66% the DSC's contain an endotherm corresponding to selenium melting at 221 °C. Each of these groups of samples is discussed in more detail in the following paragraphs.

Some of the temperatures of the thermal events in the DSC scans coincide with transitions identified in the copper-selenium phase diagram. This is especially true at higher temperatures. Since the phase diagram is based on the formation of phases from a slowly cooling melt, and these samples are from a heated metastable precursor, the phase formation at low temperatures may not align with the phase diagram. Generally, phases that have already formed will decompose at the temperature indicated on the phase diagram. The identity of phases that will preferentially form from a co-deposited precursor at specific composition, heating rate, and temperature/time are not indicated by the phase diagram.

The powder XRD scans were performed on samples after they were cooled back to room temperature. Since phase transitions will occur during this cooling process, the only phases detected after an elevated temperature anneal will be those phases remaining at ambient temperature. So, although these XRD results may identify phase creation after a thermal event, they do not actually identify the phases present at the elevated temperature.

The 50% to 60% Selenium Composition Range

Co-deposited samples with selenium composition between 50% and 60% nucleate crystalline CuSe on deposit. This was confirmed by XRD of additional co-deposited samples with compositions of 60% and 50% selenium. Figure 3.3 presents XRD data for a 51% selenium sample as-deposited and annealed in a DSC. All diffraction peaks in the as-deposited sample can be indexed to hexagonal CuSe. Samples were annealed in the DSC to identify any changes in the phases present. In this compositional region, a small endotherm is present in the DSC scan at 130 °C. A reheating of the same sample produces the same endotherm indicating that it represents a reversible process and would not be identifiable when cooled to ambient temperature. This endotherm is probably produced by the β to γ phase transition. By 180 °C, the hexagonal CuSe phase is still the only phase present, and has grown larger crystallites as indicated by the narrowing of the diffraction peaks. After annealing at 320 °C, the CuSe crystallites have significantly increased in size, but orthorhombic CuSe₂ has appeared as a minor phase as predicted by the phase diagram. The broad endotherm centered at 330 °C present in the 57% selenium DSC will be discussed in the section on selenium between 62 and 66%. The sharp endotherm present in all of the DSC scans at 377 °C is the decomposition of CuSe to $\beta(\text{Cu}_{2-x}\text{Se})$ and a selenium rich melt as expected from the phase diagram.

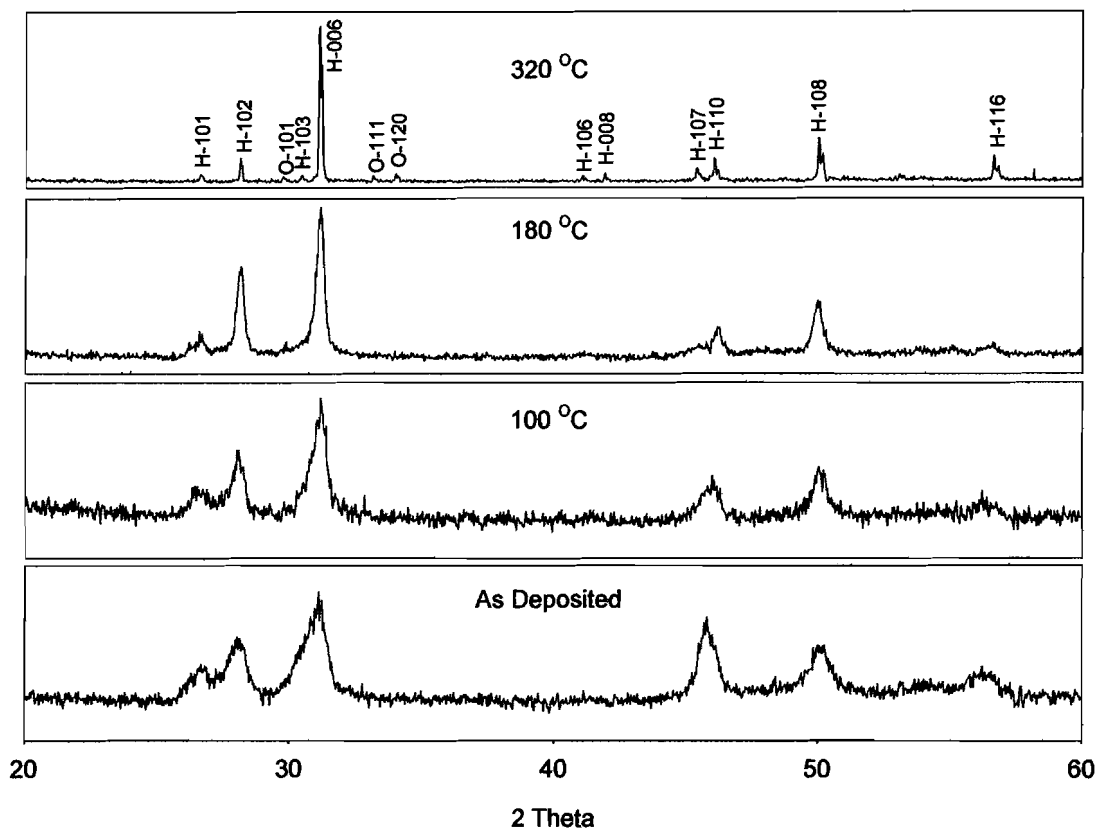


Figure 3.3. XRD data for a sample containing 51% selenium annealed to various temperatures in a DSC at a rate of 4 °C/min. Hexagonal CuSe peaks are indexed on the top graph (H-). Those prefixed with an 'O-' indicate orthorhombic CuSe₂.

The 67% to 81% Selenium Composition Range

Samples with a composition between 67 and 85% selenium are amorphous on deposit. Figure 3.4 presents XRD data on powder samples containing 68% selenium annealed in a DSC to temperatures near thermal transitions identified by the DSC scans. After the first exotherm near 110 °C multiple phases consisting of both hexagonal CuSe and cubic CuSe₂ begin to nucleate and grow. The presence of CuSe is surprising since

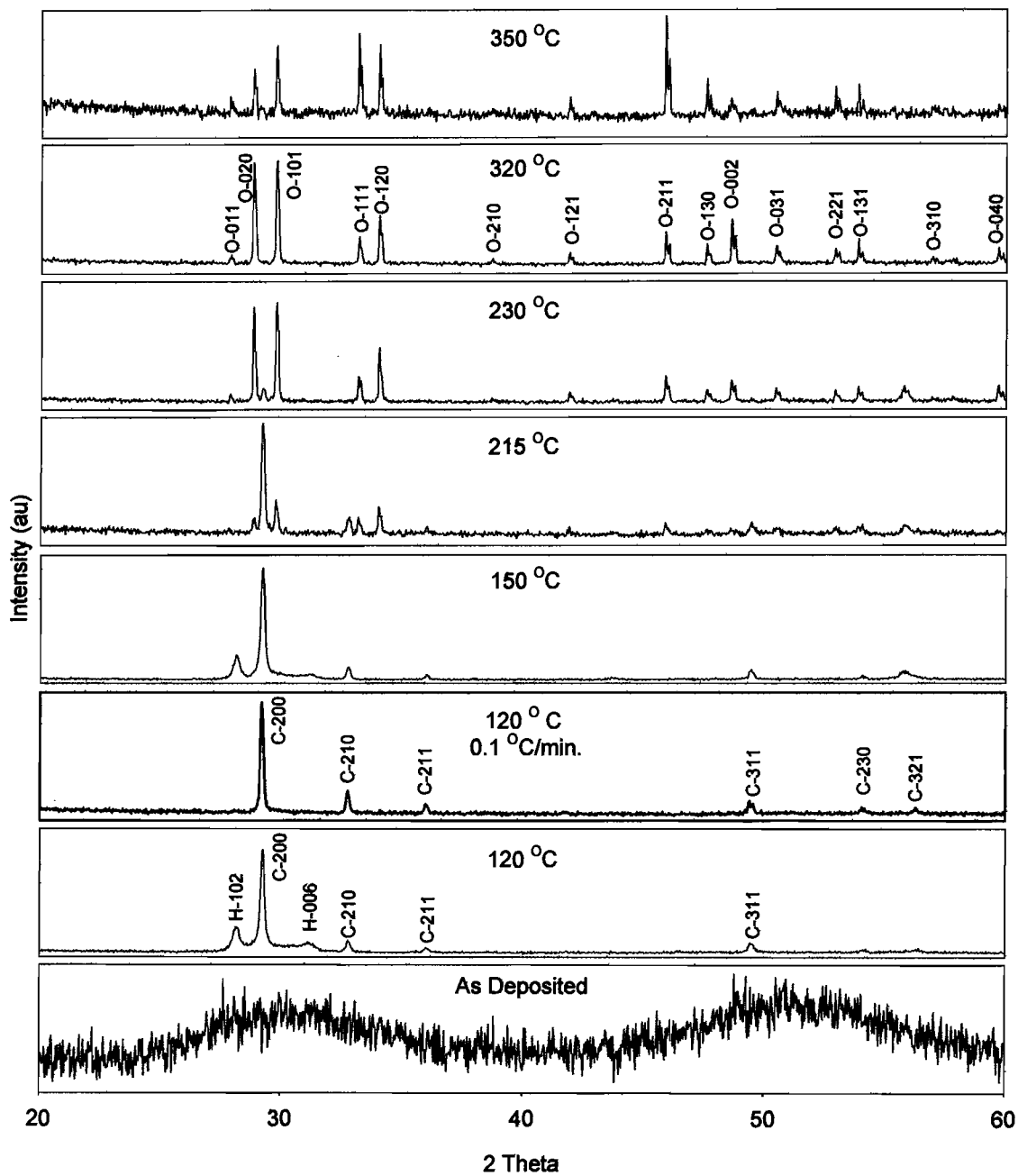


Figure 3.4. XRD data for a sample containing 68% selenium annealed to various temperatures in a DSC. Scan rates are 4 °C/min. unless otherwise indicated: H- Hexagonal CuSe, C- Cubic CuSe₂, O- Orthorhombic CuSe₂.

it is not present at this composition on the phase diagram. Additionally, since CuSe forms above 51 °C, it should be the beta phase that is nucleating. If the DSC heating rate is reduced to 0.1 °C/min., almost phase pure cubic CuSe₂ is produced. Apparently, at this composition, the nucleation of the hexagonal CuSe phase is kinetically unfavorable over that of the cubic CuSe₂ phase.

Additional samples were heated to higher temperatures at 4 °C/min. By 150 °C no significant change has occurred. By 215 °C, before the melting point of selenium, the CuSe phase has disappeared and the cubic CuSe₂ phase is converting to its orthorhombic polymorph. Although CuSe morphs into other structures, it should not decompose until 377 °C. The small CuSe crystallites appear to be less stable in this environment. The conversion of the CuSe₂ phase at this temperature is surprising since it has previously been found to be more thermally stable than the orthorhombic phase at 350 °C.¹ In that case, the material consisted of only the two CuSe₂ phases as large crystals. Perhaps the small crystal size or the presence of unreacted material is driving the conversion.

The presence of unreacted selenium in these samples is indicated by an endotherm at 221 °C, the melting point of selenium. At higher selenium percentages, this endotherm becomes more pronounced indicating more unreacted selenium. Upon the melting of the selenium, reactions now occur in a solid/liquid mixture with increased atomic diffusion. The sharp endotherm at 332 °C indicates the reversible conversion of the orthorhombic CuSe₂ to CuSe and a selenium rich melt as indicated in the phase diagram.

The selectivity of nucleation between CuSe and cubic CuSe₂ near 100 °C was further investigated with a sample containing 67% selenium. As seen in figure 3.2, the DSC at this composition has a distinctive double exotherm centered at 105 °C. Separate samples were heated at 4 °C/min. and 10 °C/min. to a temperature above the double exotherm with results presented in figure 3.5.

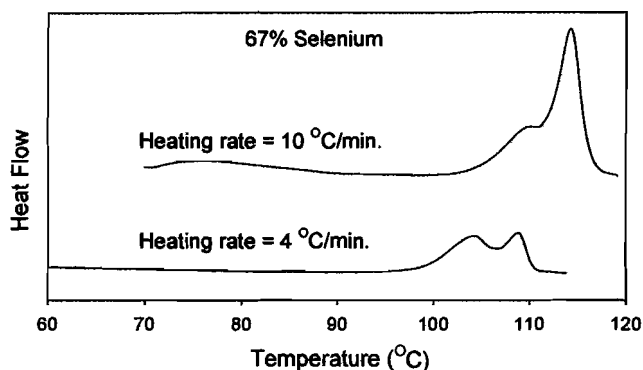


Figure 3.5. DSC scans for 67% selenium samples at heating rates of 4 °C/min. and 10 °C/min. The higher heating rate results in an increase in the magnitude of the second peak.

Figure 3.6 presents the XRD patterns that were collected on each sample. The DSC results clearly indicate that an increase in heating rate results in an increase in the magnitude of the second exotherm at the expense of the first exotherm. XRD patterns indicate that the higher heating rate resulted in nucleation and growth of more of the CuSe phase over that of the cubic CuSe₂ phase. This makes it clear that the first DSC peak represents the nucleation of cubic CuSe₂ and the second is the nucleation of CuSe.

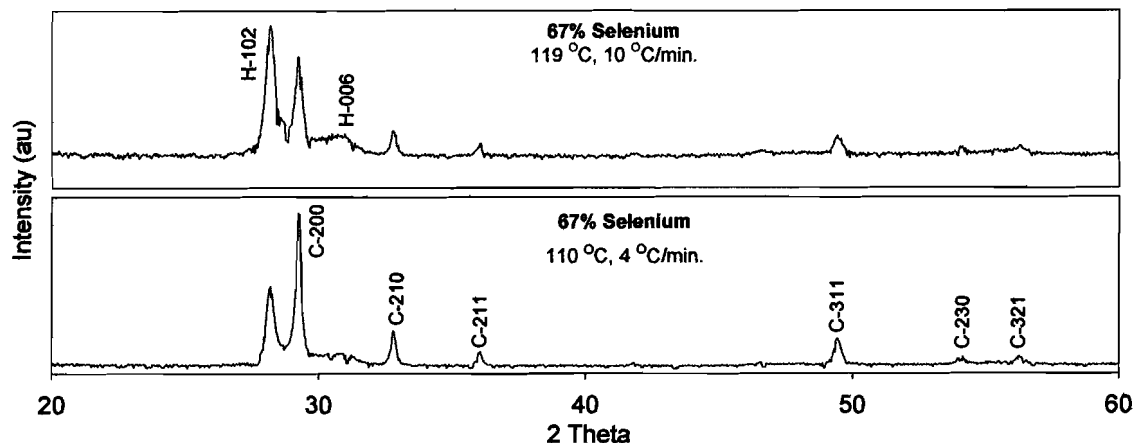


Figure 3.6. XRD patterns of 67% selenium samples heated at 4 °C/min. and 10 °C/min. The higher heating rate results in more of the CuSe phase being produced.

At the selenium rich end of this composition range, a powder sample consisting of 79% selenium was annealed at similar temperatures. XRD patterns for these annealings are presented in figure 3.7. The sample remains amorphous up to 90 °C. Like in the 68% selenium sample, both CuSe and cubic CuSe₂ nucleate when heated to 110 °C at 4 °C/min. Relative to the 68% sample, less cubic CuSe₂ is formed. This is not surprising since the composition is further from the ideal 1Cu:2Se for CuSe₂ nucleation. When the heating rate is lowered to 0.1 °C/min., the amount of CuSe is reduced but not eliminated as it was at 68% selenium. Additionally, crystalline selenium has formed, probably due to the longer time at elevated temperatures. The nucleation of hexagonal CuSe across this composition range conflicts with the phases indicated on the phase diagram and appears to be more dominant as composition deviates further from 1:2 stoichiometry. On heating to 140 °C at 4 °C/min., amorphous selenium now crystallizes. Higher temperature annealings result in the complete

conversion of cubic CuSe_2 to the orthorhombic polymorph. As seen in the 68% selenium sample, hexagonal CuSe diminishes above 140 °C.

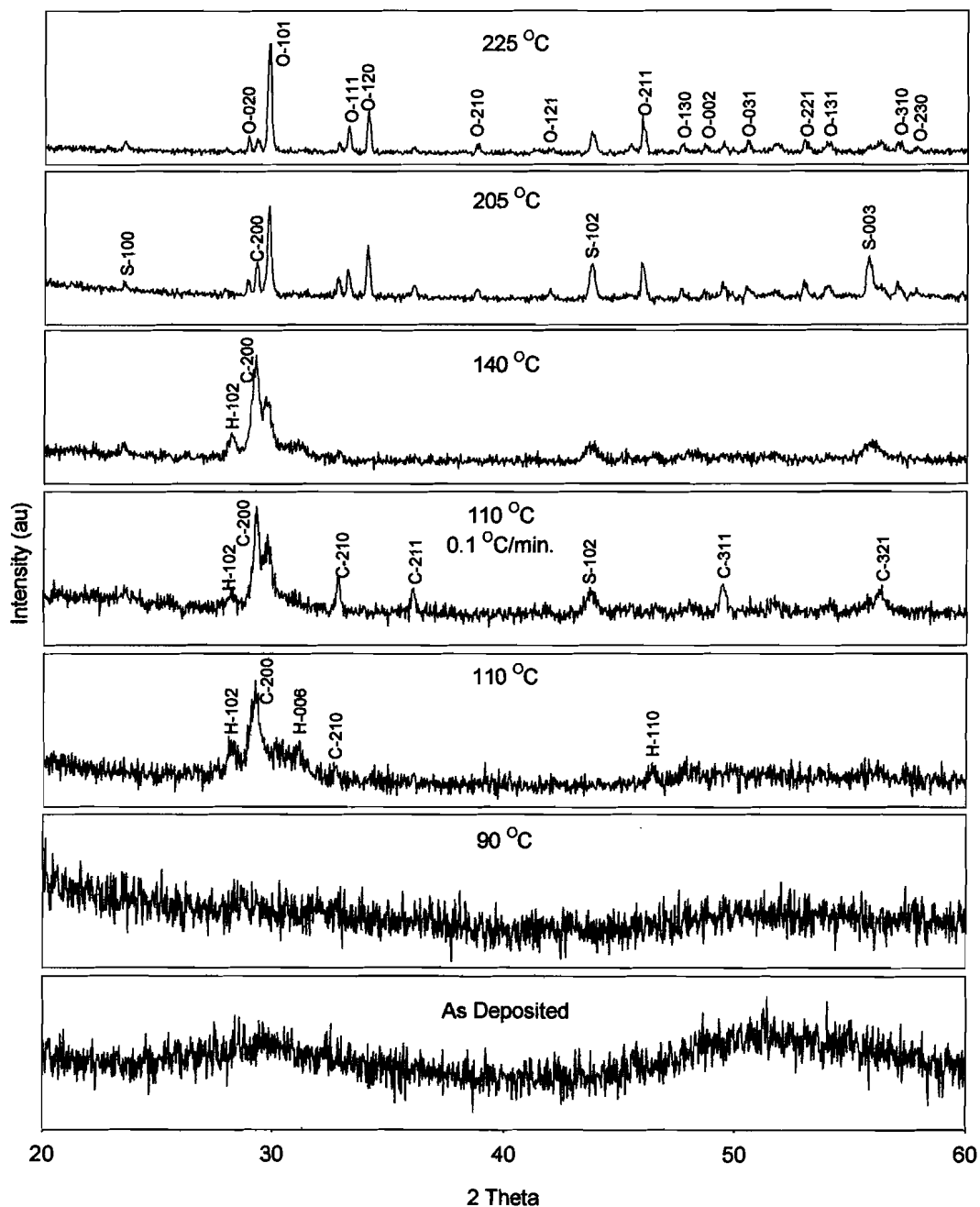


Figure 3.7. XRD data for a sample containing 79% selenium annealed to various temperatures in a DSC at a rate of 4 °C/min. unless otherwise indicated: H- Hexagonal CuSe , C- Cubic CuSe_2 , O- Orthorhombic CuSe_2 , S- Selenium.

The 62% to 66% Selenium Composition Range

Co-deposited samples with selenium composition between 62 and 66% selenium are amorphous as-deposited. Figure 3.8 presents the XRD patterns collected from

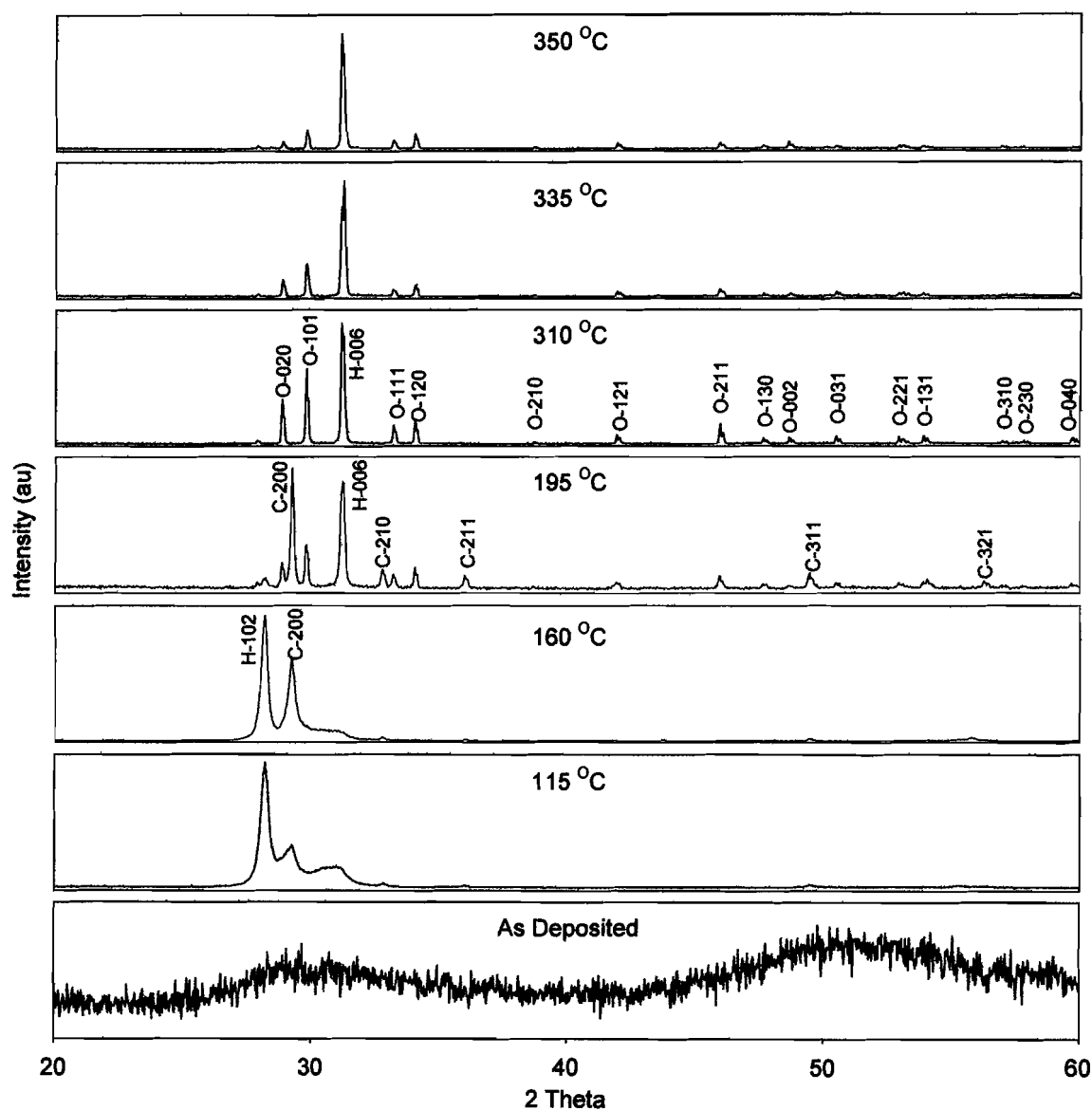


Figure 3.8. XRD data for a sample containing 64% selenium annealed to various temperatures in a DSC at a rate of 4 °C/min.: H- Hexagonal CuSe, C- Cubic CuSe₂, O- Orthorhombic CuSe₂.

powder samples annealed at temperatures up to 350 °C. Like the selenium rich compositions containing more selenium, most of these samples produced both CuSe and cubic CuSe₂ on heating to 115 °C. In this composition range, however, the sharp endotherm at 332 °C is replaced by a broad endotherm. A second DSC scan of the same sample to 400 °C produced the same endotherm indicating that it is a reversible process. XRD patterns collected by Murray¹ showed this transition to be the slow conversion of orthorhombic CuSe₂ to CuSe and selenium. The process by which this conversion occurs appears to be different for samples containing excess liquid selenium and those in a completely solid state.

For the selenium rich compositions of the copper-selenium binary system, the composition near 66% selenium is unique. As shown in figure 3.9, only cubic CuSe₂

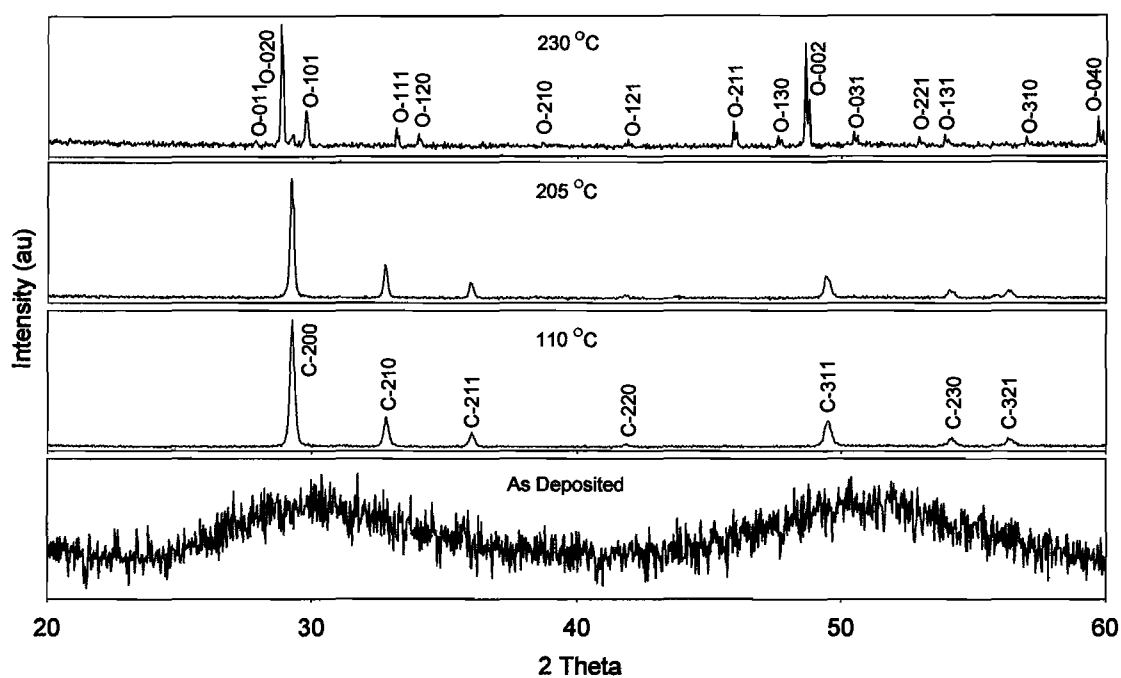


Figure 3.9. XRD data for a sample containing 66% selenium annealed to various temperatures in a DSC at a rate of 4 °C/min.: C- Cubic CuSe₂, O- Orthorhombic CuSe₂.

forms during the first exothermic event between 100 and 110 °C. Since only one phase forms near 110 °C, DSC data was collected at heating rates from 0.1 to 10 °C/min. to determine the activation energy for cubic CuSe₂. Non isothermal DSC data can be analyzed using a Kissinger analysis. In a Kissinger analysis, the activation energy is obtained from the peak temperature of the DSC exotherm, T_p , as a function of thermal scan rate Q :²⁰

$$\frac{d \ln[Q/T_p^2]}{d[1/T_p]} = \frac{-E_{\text{crystallization}}}{R}$$

where R is the gas constant. Graphing $\ln[Q/T_p^2]$ versus $1/T$ gives a straight line with a slope equaling $-E/R$ from which the activation energy for the nucleation and growth process is extracted.²⁰ DSC data was collected on samples containing 66% selenium at heating rates of 0.1, 1, 4, and 10 °C/min. to 110 °C. Each sample was then characterized by XRD to confirm that only the cubic CuSe₂ phase was present and to quantify the lattice parameter of the crystallites. The Scintag software was used to locate the peak centers. The lattice parameter calculated from this data agreed with the published value of 6.116 angstroms.¹ The DSC data was plotted (figure 3.10) and the activation energy extracted. The activation energy for nucleation was determined to be 1.6 eV.

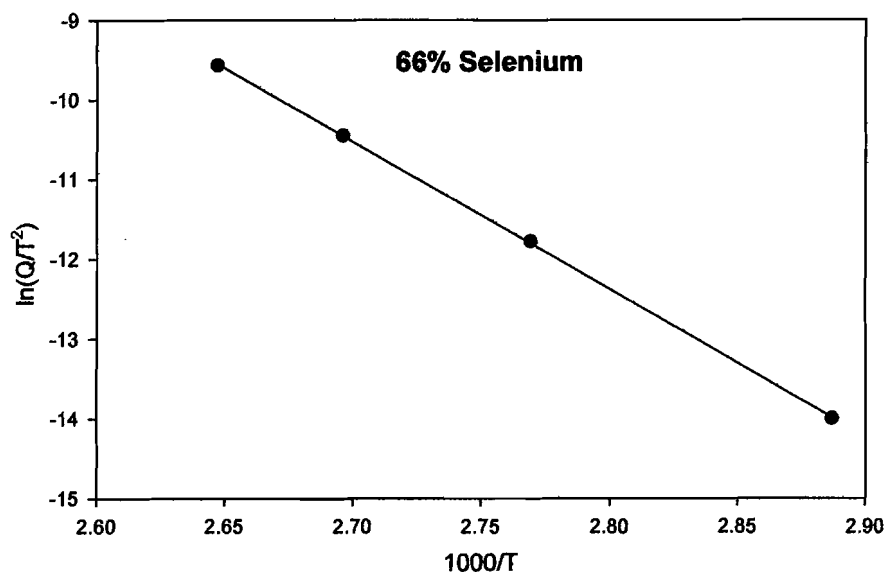


Figure 3.10. Kissinger plot used to derive the activation energy for nucleation of cubic CuSe_2 . DSC heating rates were 0.1, 1.0, 4.0, and 10 °C/min. The arguments of the logarithm were made unitless by dividing by the constant T_0^2/Q_0 where T_0 is 1000 K and Q_0 is 1 deg./min.

Copper selenide compounds have been known to form and reorder over extended time periods under ambient conditions. Murray found that new XRD reflections had appeared in a seven year old sample of CuSe indicating a slow ordering process.¹ More recently Ohtani produced Cu_3Se_2 in an ambient temperature solid state reaction between $\alpha\text{-CuSe}$ and $\alpha\text{-Cu}_2\text{Se}$ over a span of several days.²¹ XRD patterns were collected on three powder samples that were stored in vials at ambient temperature for 44 months. The sample consisting of 72% selenium remained amorphous and the sample at 57% selenium remained unchanged with the presence of small CuSe

crystallites. XRD patterns are presented in figure 3.11 for a sample consisting of 64% selenium that had nucleated and grown both cubic CuSe_2 and CuSe with cubic CuSe_2 being the dominant phase.

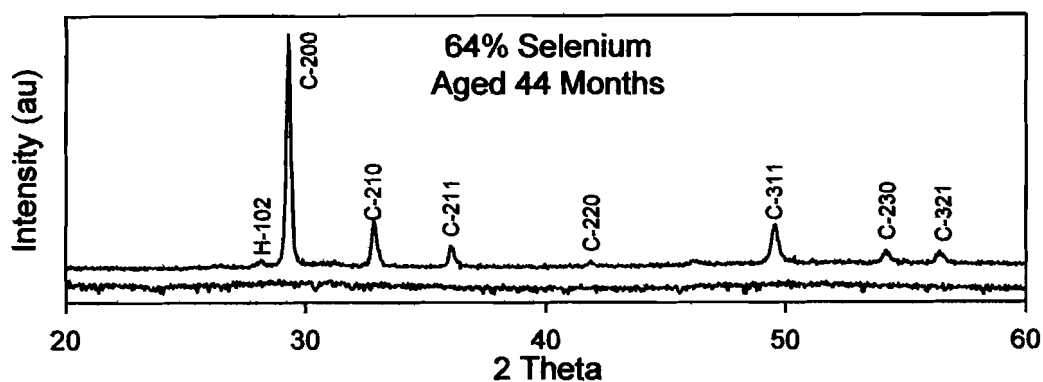


Figure 3.11. XRD patterns for a 64% selenium sample soon after deposition and 44 months later.

Summary

The most surprising result of this research has been the low temperature nucleation of cubic CuSe_2 over its thermodynamically stable orthorhombic polymorph. The nucleation of the cubic phase occurred over a wide range of selenium rich compositions. The composition containing 66% selenium distinguished itself by forming phase pure cubic CuSe_2 at heating rates up to $10\text{ }^\circ\text{C}/\text{min}$. At compositions close to the stoichiometrically ideal 1:2 the cubic CuSe_2 phase could be preferentially nucleated over CuSe via kinetic control by slow heating rates. This would imply that the CuSe_2 phase nucleates first on heating. Additionally the cubic phase showed lower

thermal stability than previously reported, converting to the orthorhombic phase near 200 °C.

Another surprise was the broad compositional range over which hexagonal CuSe formed. In the phase diagram, the CuSe phase is restricted to compositions with less than 67% selenium. If CuSe₂ is the first phase to form at compositions above 67%, then the remaining material becomes enriched in selenium, driving the remaining unreacted phase further from the ideal 1:1 stoichiometry of CuSe. CuSe appears to be kinetically stable at compositions above 67% selenium but decomposes on annealing above 140 °C.

CHAPTER IV
THE EFFECT OF ELEMENTAL STACKING ORDER AND LAYER
THICKNESS IN CONTROLLING THE FORMATION
KINETICS OF COPPER INDIUM DISELENIDE

Introduction

Generally speaking, most inorganic solids are produced from a high temperature reaction of the granular component elements. A sufficiently high temperature must be achieved not only to react the initial components, but also any intermediate compounds formed at the interface of the precursor particles and those formed by the precursors interface with the liquid phase. Controlled cooling and annealing programs are used to impart properties in the solid that deviate from the thermodynamically stable phases. Among these, macroscopic properties such as number and identity of phases, grain size, phase segregation, crystal orientation, and a host of other properties are sought to produce a material with the desired properties.

To access new metastable phases or to create thermodynamically stable phases at lower temperatures, a rational approach utilizing control of composition, diffusion, and phase nucleation needs to be used. One such approach is the creation of a stacked

elemental layer that will inter-diffuse to form an amorphous intermediate precursor. Judicious selection of annealing conditions allows the elemental layers to inter-diffuse before nucleation occurs.

In a simple binary thin film, there is only one type of interface between the two elemental layers, and of course the front and back surfaces. For these systems, a 'critical thickness' has been defined as the transition point between complete inner diffusion before nucleation, and phase formation at the interface before diffusion is complete. Either situation may be desirable depending on the targeted phases(s) and structure. Nucleation at an interface can result in a preferred alignment of the growing crystallites. Complete diffusion before nucleation can be utilized to create a metastable amorphous intermediate that is further processed to form a crystalline phase.

Elemental layer interaction becomes more complex when three elements are deposited as thin films. There are now up to three elemental interfaces. Ternary layering has previously been used to form superlattices of two different binary phases with the common element to both phases separating the other two elements.^{1,2,3} If one wishes to form a single phase from an amorphous precursor consisting of the three elements, then the layer thickness is limited to prevent nucleation of binary compounds before diffusion is complete. The situation becomes even more complicated when one wishes to form an amorphous, homogeneous precursor from which to nucleate the desired phase. The question becomes, why not just co-deposit the three elements to form the amorphous precursor. Indeed this process will work, assuming that a binary or ternary phase does not nucleate under ambient deposition conditions. In addition, the

energetics of the annealing must be conducive to nucleation of the ternary over those of the possible binary compounds.

The desire for an amorphous precursor for the copper indium diselenide system has led to an investigation of how the order and thickness of elemental selenium, indium, and copper layers affect nucleation and growth of copper indium diselenide. For this material system, co-deposition of the three elements close to the 1Cu:1In:2Se stoichiometry resulted in nucleation of CIS and other unidentified crystalline phases. Additionally, depositing the elements in a simple repeat pattern of Se:In:Cu at repeat length scales of 20 and 60 angstroms resulted in nucleation of CIS and a CuSe phase. A more complex deposition order stabilizing the copper and selenium while separating the indium from the copper was developed to suppress the nucleation of binary and ternary phases.

Experimental

The films described in this chapter were deposited in a custom built high vacuum chamber described in chapter II. The composition of all samples was determined using the thin film technique for microprobe described in chapter II. XRD and XRR patterns were collected on either the Scintag XDS 2000 or the Bruker D8 Discover Diffractometers. No distinction will be made as to which one was used to collect each pattern. XRD patterns were compared to ICDD powder diffraction file patterns⁴ for identification purposes. Using the Bragg equation, the position of the low order reflectivity peaks in the XRR data was used to calculate layer repeat thickness.

Indium Selenium Layers

As a prelude to investigating the layering of selenium, indium, and copper, the indium-selenium and copper-selenium binary layered systems were investigated. To make smooth, amorphous films, it is important to understand the interactions of the metals with the selenium at short length scales.

A series of indium-selenium binary films were deposited to calculate the selenium and indium layer thicknesses. Samples were made by depositing 20 repeat sets of the two elements. Indium was deposited from an e-beam gun and selenium from an effusion cell. The desired deposition thickness of the selenium layer was held constant for all films while varying the layer thickness of indium in each sample. Figure 4.1 presents the XRR patterns for the binary thin films. As indicated by the lack of Kiessig fringes at higher 2θ , films with indium thicknesses above 15 angstroms appear significantly rougher.

Total repeat thickness was calculated from the Bragg equation using the reflection peaks from the bottom five patterns. The total repeat thickness was plotted against the indicated indium thickness. Indicated thickness is not the same as actual layer thickness due to a difference in source to crystal monitor and source to substrate distance (tooling factor), though the correction is linear. The Y-intercept of a linear regression line fitted to the data denotes the total repeat thickness with effectively no indium layer, only the selenium layer. The selenium layer thickness was calculated to be 63 angstroms. Subtracting 63 angstroms from each of the total repeat thicknesses gives the true indium thickness for each sample.

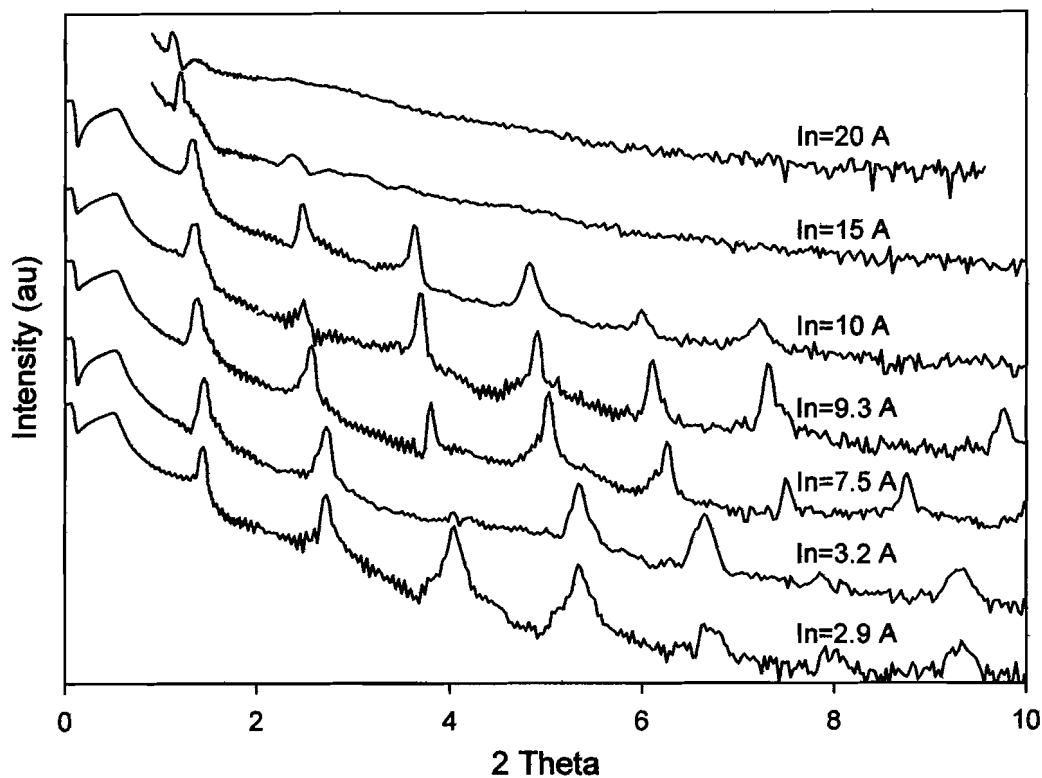


Figure 4.1. X-ray reflectivity scans of indium selenide layered thin films.

Figure 4.2 presents the indium layer thickness versus both total repeat thickness and the indium to selenium atomic ratio as determined by microprobe. The indium layer thickness for the two thickest films was calculated from the linear regression data and plotted as a visual aide. Along with layer thickness, the ratio of indium to selenium is plotted and referenced by the right hand Y-axis.

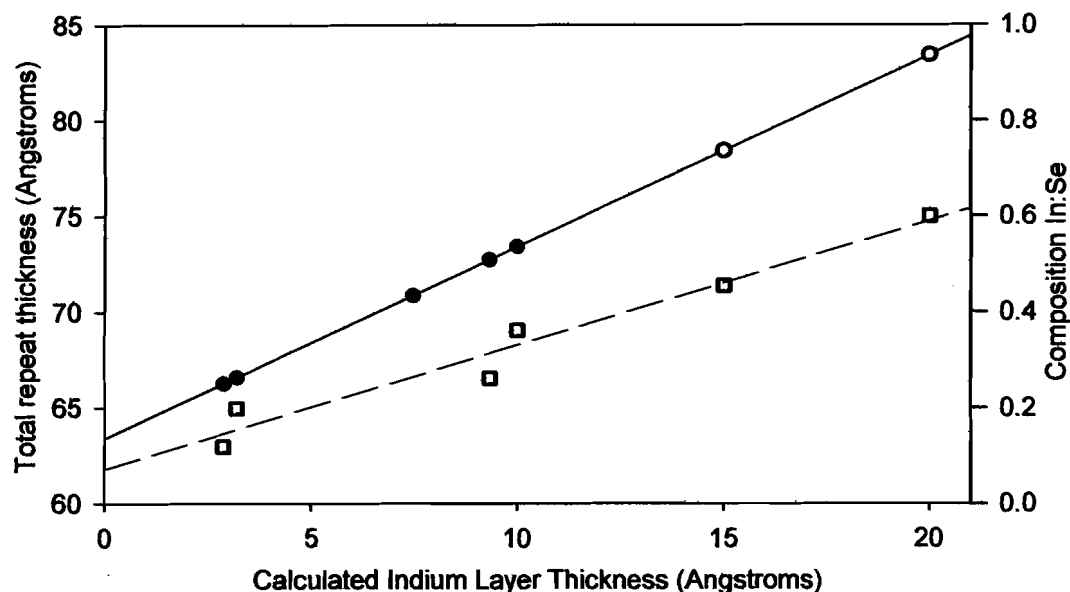


Figure 4.2. Total repeat thickness (circles) and composition (squares) vs. indium layer thickness.

XRR patterns of the two indium-selenium films with 15 and 20 angstrom indium layer thicknesses shows them to be significantly rougher as indicated by the lack of high order Bragg reflections. XRD patterns in figure 4.3 of the three films with the thickest indium layer show the formation of crystalline indium when the indium layer thickness has reached 20 angstroms. The full width at half the maximum intensity of the indium (101) peak was measured and the Debye-Scherrer equation used to calculate the crystal size as over 200 angstroms. The indium crystallites have grown larger than the repeat thickness of the indium-selenium repeat layers revealing the source of the interfacial roughness. To prevent inner mixing of the elements in a Cu-In-Se thin film, the indium layer must be thinner than 15 angstroms to prevent nucleation of elemental indium.

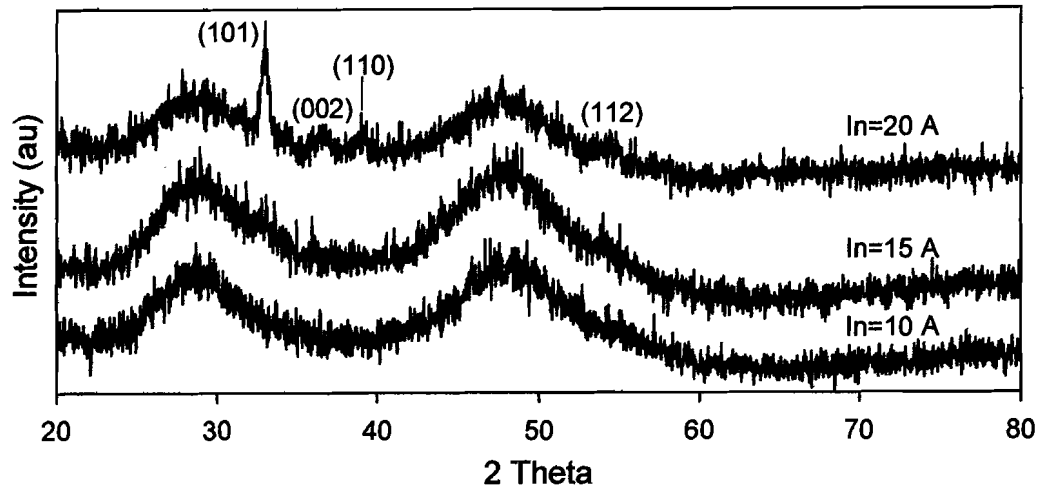


Figure 4.3. Indium crystallization at layer thicknesses above 15 angstroms.

Copper Selenium Layers

The copper selenium binary system was investigated to determine the conditions of composition and repeat thickness that would produce an amorphous intermediate film. A set of 11 binary copper-selenium layered films were deposited to investigate the effect of repeat thickness and composition on ambient temperature nucleation and growth of crystalline phases. Films were simultaneously deposited on quartz for XRD and silicon for XRR and composition analysis. The nucleation of crystallite phases at the copper selenium interface will produce both roughness in the CIS layers and produce a binary phase that would need to be thermally annealed to produce the CIS. Nominally, four compositions were deposited at three repeat thicknesses with both the selenium and copper deposition times varied to achieve the desired composition and repeat thickness.

Figure 4.4 presents the XRR patterns for the sample films deposited on silicon. The repeat thickness for the top two patterns was calculated from the position of the first order reflections. All other repeat thicknesses were approximated from these two values. The black dots on the patterns show the location of the highest order Kiessig fringe visibly discernable. Diminishing of the Kiessig fringes correlates with film roughness. The films with selenium composition above 65% are significantly smoother compared to those with less selenium.

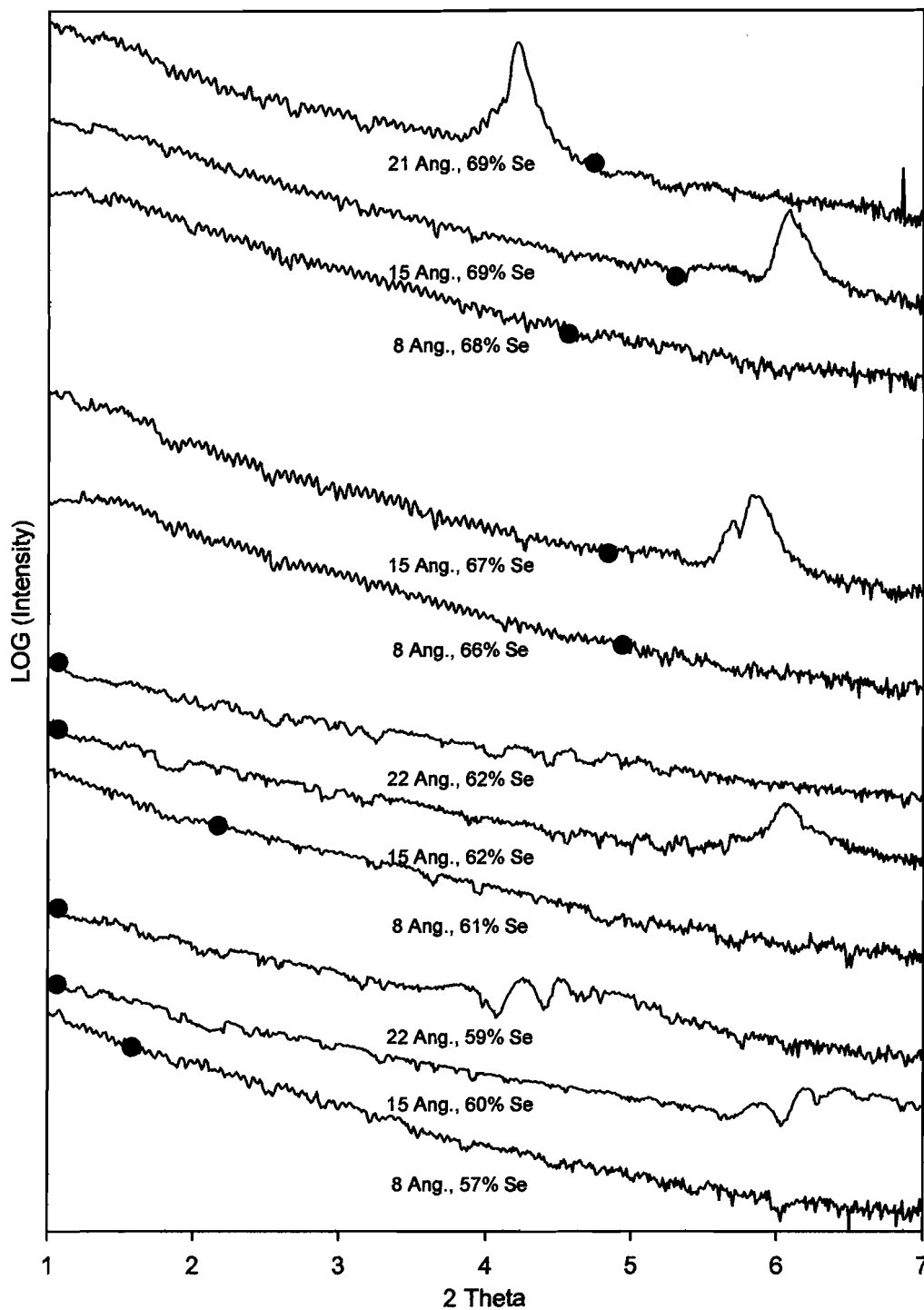


Figure 4.4. XRR data for Cu-Se layered films at compositions between 57 and 69% selenium at three different repeat thicknesses. The solid dots indicate the highest angle of discernible Kiessig fringes.

Figure 4.5 presents the XRD data for these same samples. Taken together, the XRR and XRD patterns present an informative story of what is happening at the compositions and repeat thicknesses of interest. In the films with a selenium concentration below 62%, CuSe is nucleating and growing under ambient conditions at all repeat thicknesses. This crystalline growth is disrupting the elemental layering and is the cause for the general weakness of both the XRR first order reflections and Kiessig fringes. The sample composed of 62% selenium and a repeat thickness of 15 angstroms has crystalline CuSe present and layering still present as indicated by the first order diffraction peak. Although the first order diffraction peak indicates the presence of some layering, the Kiessig fringes have been lost due to film roughness. This conflicting result would imply that there are two distinct regions intermixed within the film. The films with selenium compositions above 66% selenium are distinctly smoother as indicated by the presence of the first order reflections and Kiessig fringes extending out to about 5 degrees 2 theta.

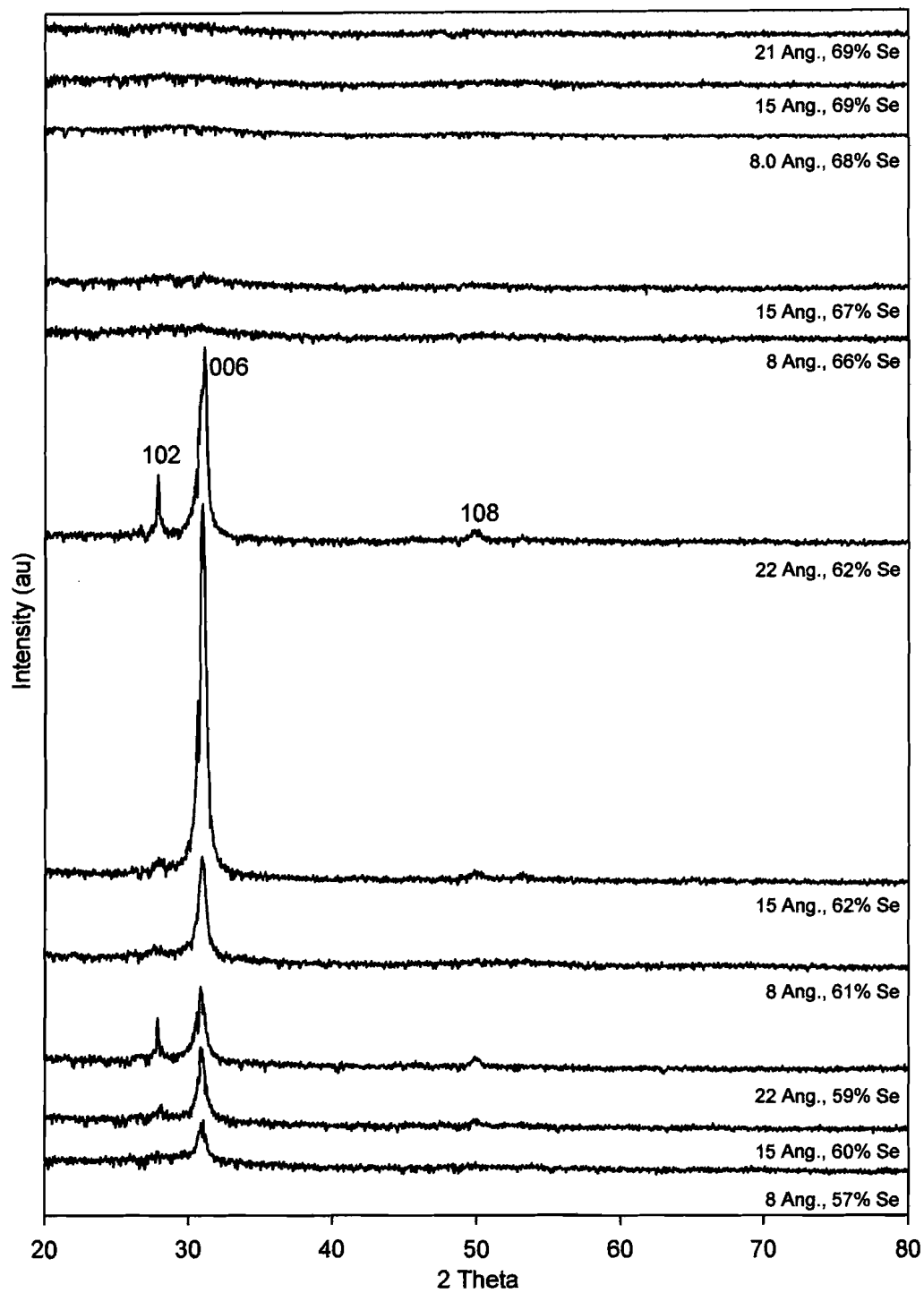


Figure 4.5. XRD patterns for layered copper-selenium samples. Nucleation of CuSe occurs for compositions containing less than 65% selenium.

Throughout a broader investigation of the copper-selenium phase space, additional copper-selenium films were deposited, both layered and co-deposited. A summary of their propensity toward nucleation as-deposited is presented in figure 4.6. The distribution of the data indicates that increased layer thickness or a reduction in the selenium percentage drives the system toward nucleation and growth of hexagonal CuSe. At a large layer thickness, inter-diffusion of the copper and selenium is

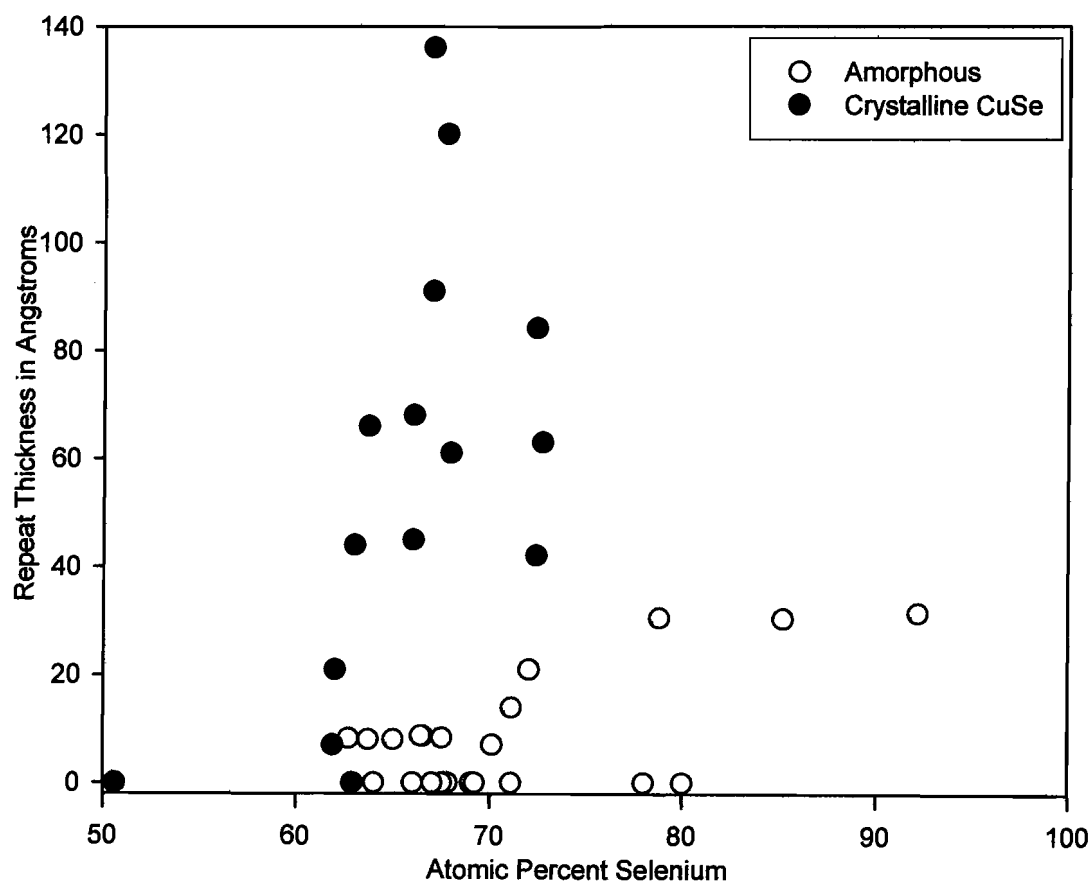


Figure 4.6. Summary of XRD results for copper-selenium layered and co-deposited films. Films with less selenium or larger repeat thicknesses will nucleate the CuSe phase.

incomplete resulting in a gradation of composition through the sample. If the elemental composition is close to 1:1 for a sufficiently large region, nucleation and growth occurs.

Copper-Indium-Selenium Layers

Multiple films containing copper, indium, and selenium layers at differing layer thicknesses, composition, and elemental order were deposited on both quartz and silicon. Figure 4.7 depicts three of the four deposition strategies, the other being simple

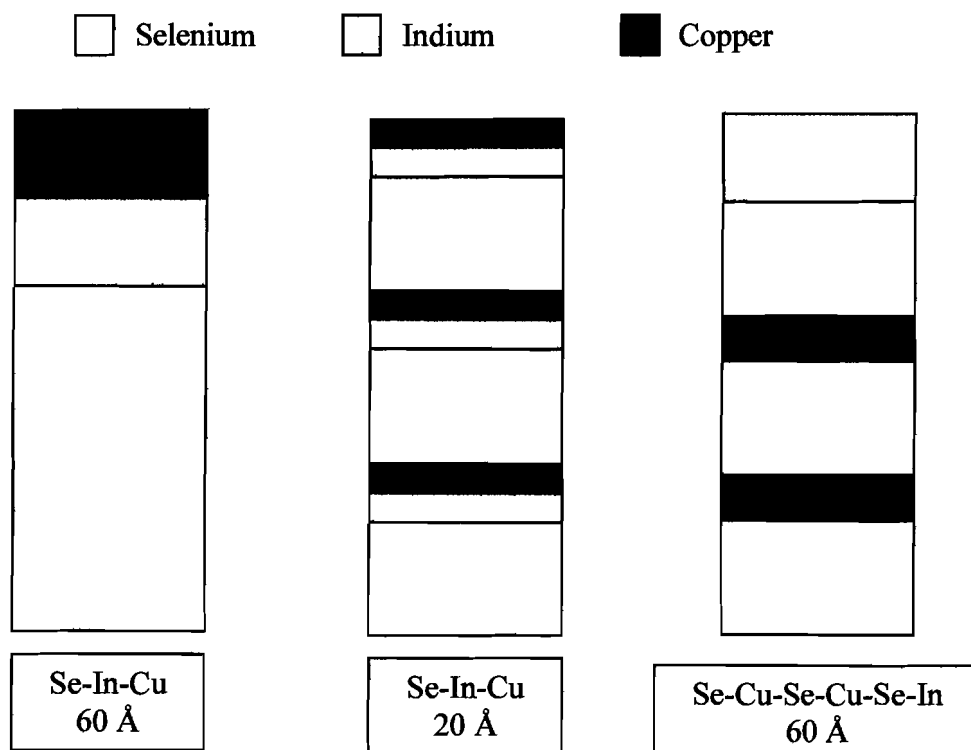


Figure 4.7. Schematic representations of the three repeat layering schemes used to investigate the effect of layer repeat thickness and order (co-deposition not pictured).

co-deposition. The first two are simple stacking of the three elements at a 60 angstrom and 20 angstrom repeat thickness. The third structure sandwiches the copper between three selenium layers, isolating the copper from the indium. The total thickness of all the samples ranged from 0.2 to 1 micron.

Figure 4.8 summarizes the results of these depositions. The axes are identified as the stoichiometric ratio of copper (X-axis) and indium (Y-axis) to 2 seleniums. The diagonal line represents compositions along the $\text{In}_2\text{Se}_3\text{-Cu}_2\text{Se}$ tie line. The only amorphous films exist for selenium rich compositions using the Se-Cu-Se-Cu-Se-In stacking order. Each layer order/thickness will be discussed in further detail below.

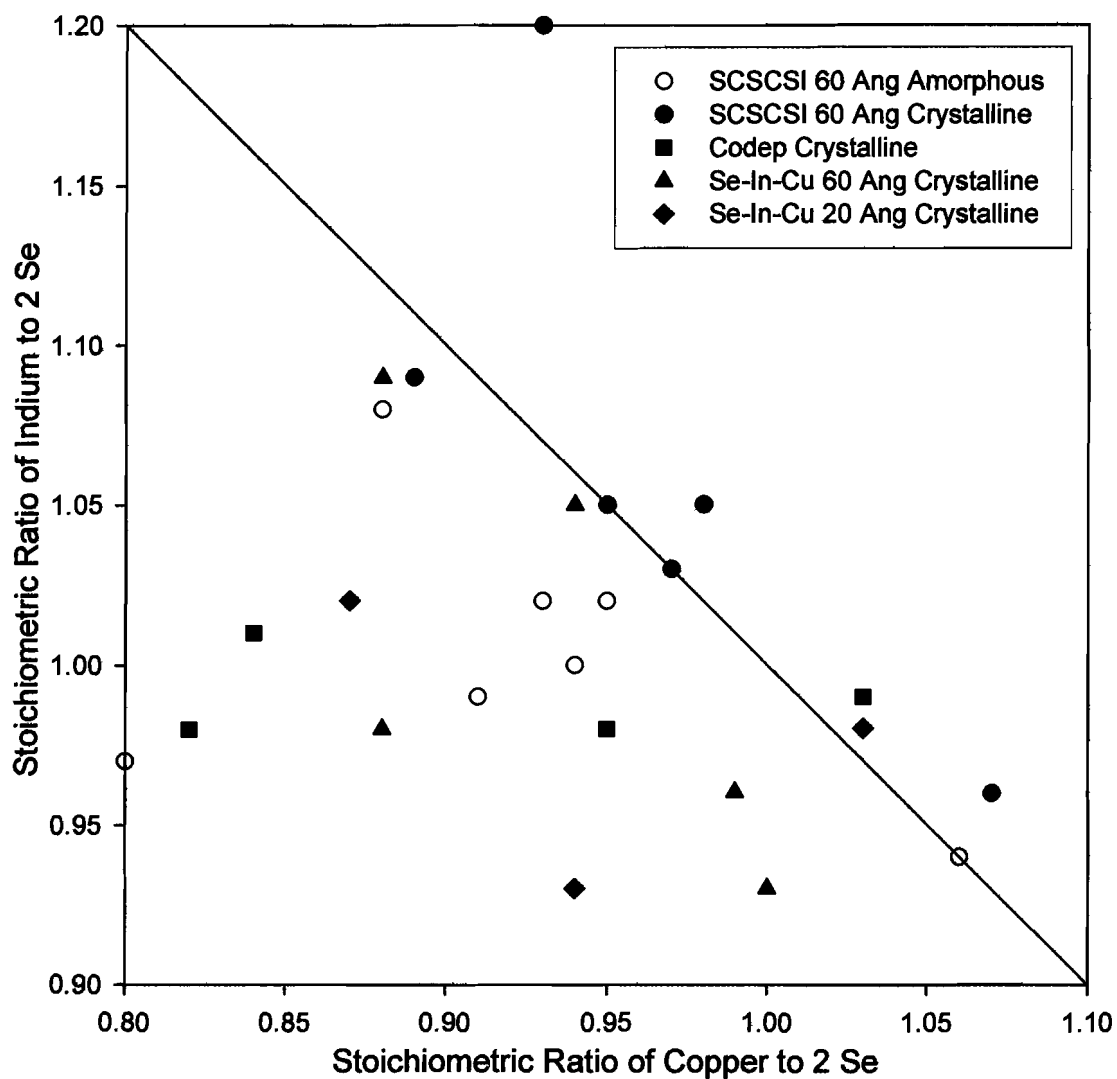


Figure 4.8. Summary of deposition results indicating the stacking order/thickness and composition resulting in as-deposited nucleated and amorphous films. The diagonal line represents compositions along the In_2Se_3 - Cu_2Se tie line.

Co-Deposited Selenium-Indium-Copper

Four thin films composed of co-deposited copper, indium, and selenium were deposited onto quartz. Each film was approximately 3000 angstroms thick as approximated by microprobe. The XRD patterns of the as-deposited films are presented in figure 4.9. All four films show the presence of crystalline CIS and an unidentified secondary phase. The samples with compositions closer to the 1:1:2 stoichiometry have more intense diffraction peaks indicating a higher level of crystallinity. Nucleation of CIS in the co-deposited films indicates that simple co-deposition will not produce the desired amorphous precursor.

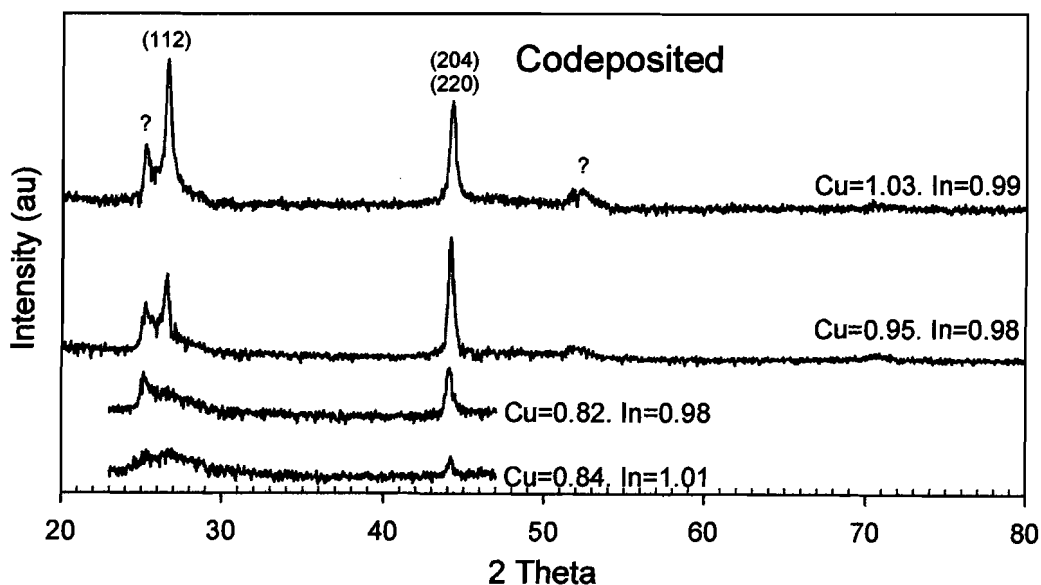


Figure 4.9. XRD patterns for copper, indium, and selenium co-deposited onto quartz to a depth of approximately 3000 angstroms.

60 Angstrom Repeat Layered Selenium-Indium-Copper Films

From the results of the co-deposited samples, it became obvious that it was necessary to prevent inner mixing of the three elements to produce an amorphous precursor. Several films were deposited with the deposition order Se-In-Cu onto silicon substrates. The XRD patterns for films composed of Se:In:Cu with a 60 angstrom repeat thickness are presented in figure 4.10. All films with this repeat thickness were crystalline as-deposited. At this large repeat thickness, diffusion of copper and selenium produced a region of the necessary composition and thickness to nucleate

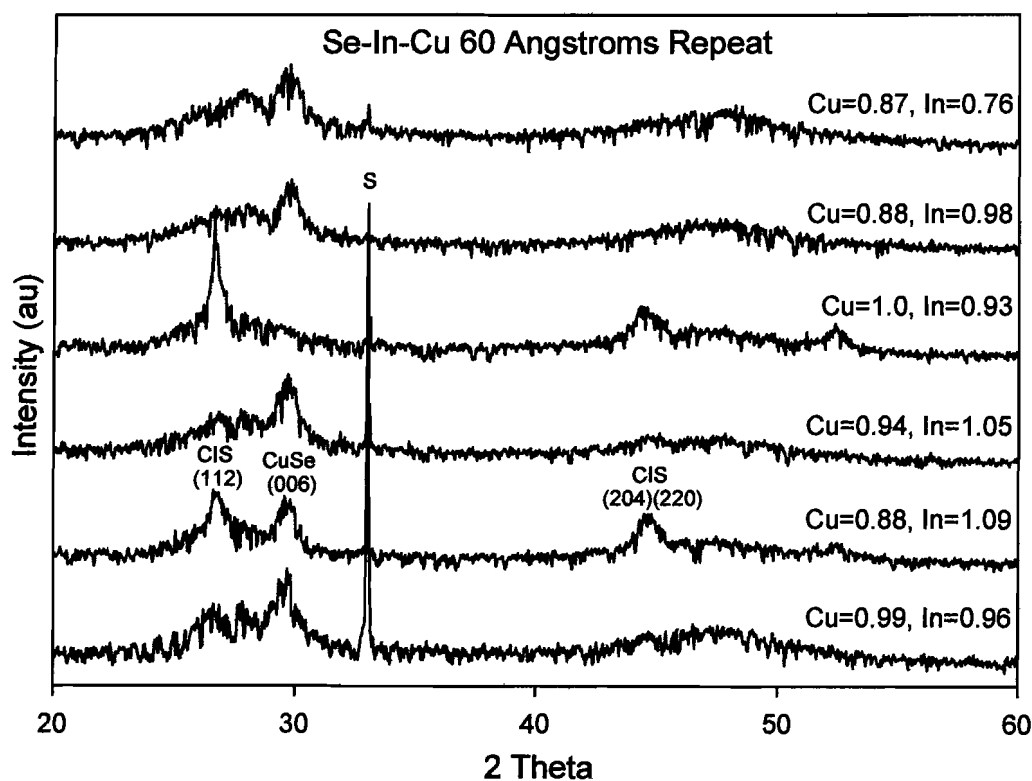


Figure 4.10. XRD scans for Se:In:Cu films with a 60 angstrom repeat thickness. Composition of each film is displayed on the right above each XRD pattern. The peak at 33 degrees is from the substrate.

hexagonal CuSe as indicated by the presence of its (006) peak. Additionally, XRD peaks consistent with crystalline CIS are present in samples with compositions close to 1Cu:1In:2Se. The CIS ternary phase may have been produced by simple diffusion of the three elements, or by the disruption of the elemental layers by the growth of the CuSe.

20 Angstrom Repeat Layered Selenium-Indium-Copper Films

To prevent the conditions under which the CuSe binary formed, the repeat thickness was reduced to 20 angstroms while maintaining the same deposition order. Figure 4.11 presents the XRD patterns for the as-deposited samples. As expected from the layered binary Cu-Se samples, reduction of the repeat thickness eliminated the conditions under which CuSe could nucleate. However, at this thin repeat thickness, the three elements came into contact and the ternary CIS phase nucleated.

At large repeat thicknesses, the copper and selenium layers diffuse and nucleate CuSe. At short repeat thicknesses, the copper, indium, and selenium are in intimate contact and nucleate CIS similar to the co-deposited samples, but without the unidentified second phase. The key to forming an amorphous intermediate is to maintain a smooth layering to prevent the three elements from coming into contact with each other while preventing a region of copper and selenium forming near the 1:1 stoichiometry.

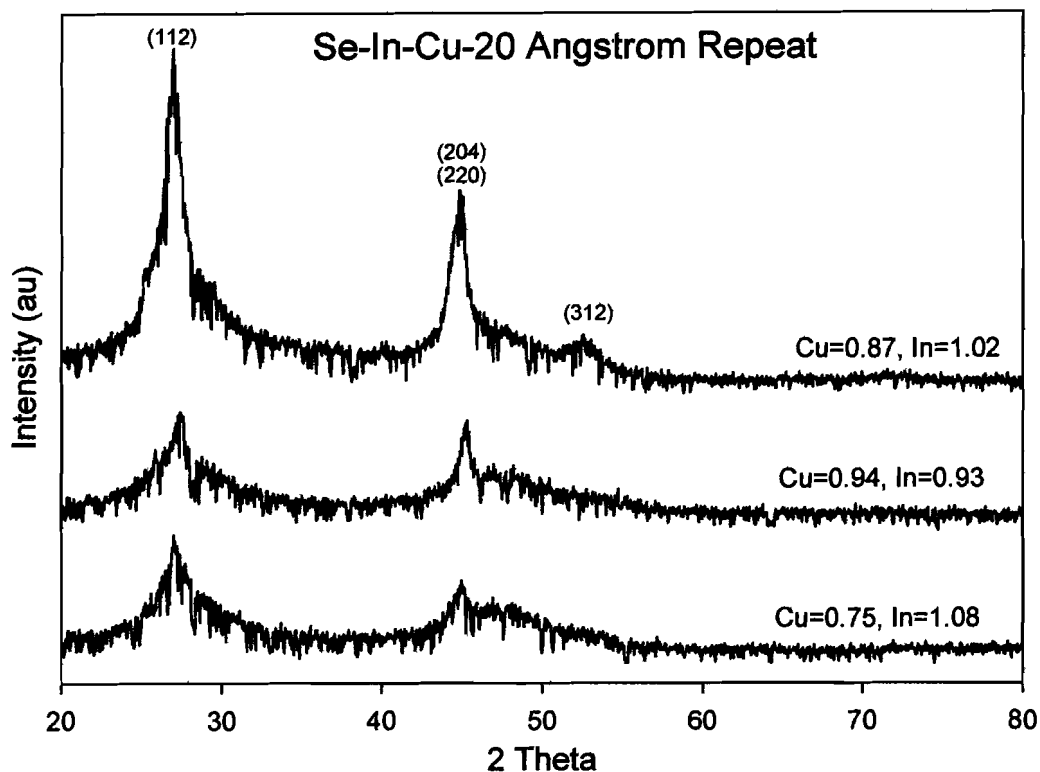


Figure 4.11. XRD patterns for thin film samples deposited in the order Se:In:Cu with a 20 angstrom repeat thickness.

60 Angstrom Repeat Layered Se-Cu-Se-Cu-Se-In Films

To meet these requirements, a new deposition order was used (Se-Cu-Se-Cu-Se-In) at a repeat thickness of 60 angstroms. For this repeat pattern, the copper and selenium layers are thin enough to rapidly diffuse forming a 1:2 Cu:Se composition that will not nucleate CuSe. The indium layer is only 10 angstroms thick, preventing the crystallization of the indium. In addition, the time required for copper diffusion through the selenium layer next to the indium prevents all three elements from contacting each other. Figure 4.8 summarizes the compositions using this deposition strategy that

resulted in an amorphous film or one that nucleated CIS on deposit and figure 4.12 presents the XRD patterns for the amorphous Se-Cu-Se-Cu-Se-In films and one XRD pattern for a crystalline thin film for comparison purposes. Films containing copper and indium in excess of the $\text{In}_2\text{Se}_3\text{-Cu}_2\text{Se}$ tie line were crystalline while those with excess selenium were generally amorphous.

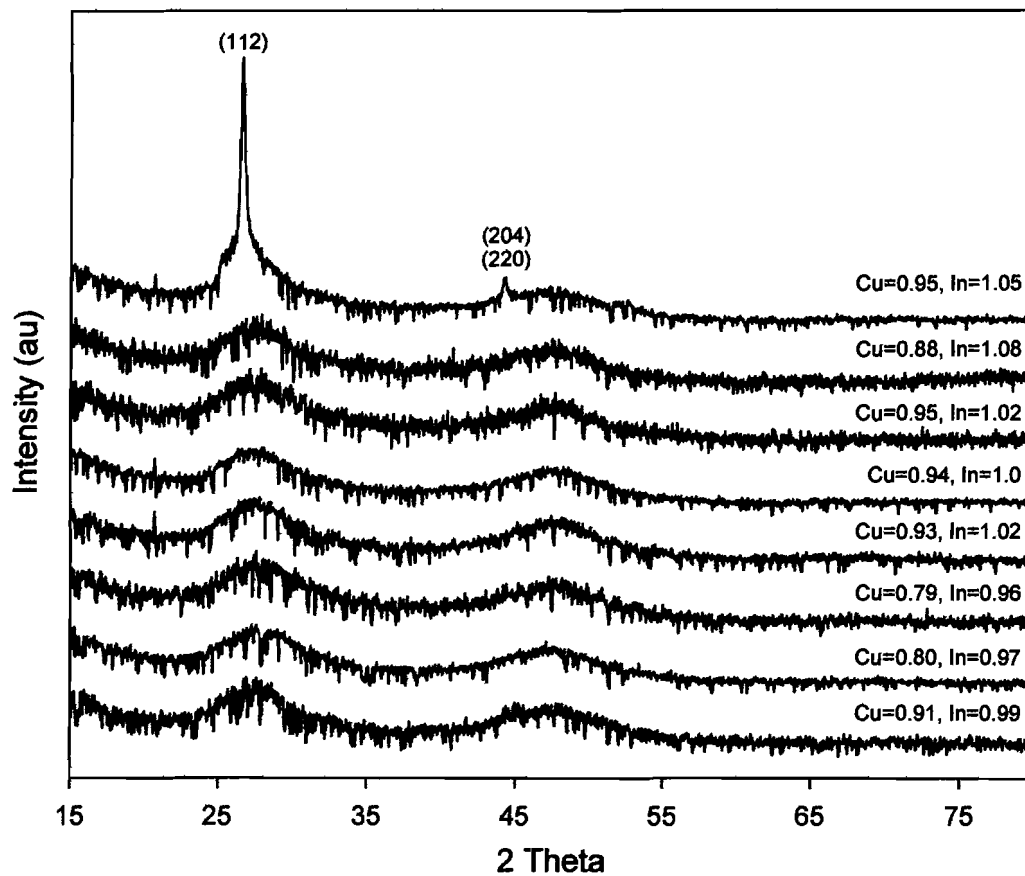


Figure 4.12. XRD patterns for the as-deposited Se-Cu-Se-Cu-Se-In films deposited at a repeat thickness of 60 angstroms and 5000 angstroms total thickness. The bottom seven patterns represent the samples that were amorphous on deposit. The top pattern is presented as an example of a film that crystallized.

The position of the third order diffraction peak on the XRR patterns for the amorphous Se-Cu-Se-Cu-Se-In films presented in figure 4.13 were used to calculate the thickness of the Se-Cu-Se-Cu-Se-In repeating layer. Repeat thickness ranged from 58 to 63 angstroms. The presence of the three orders of Bragg peaks indicates that the layering of the thin film, though highly inter-diffused, is still in tact.

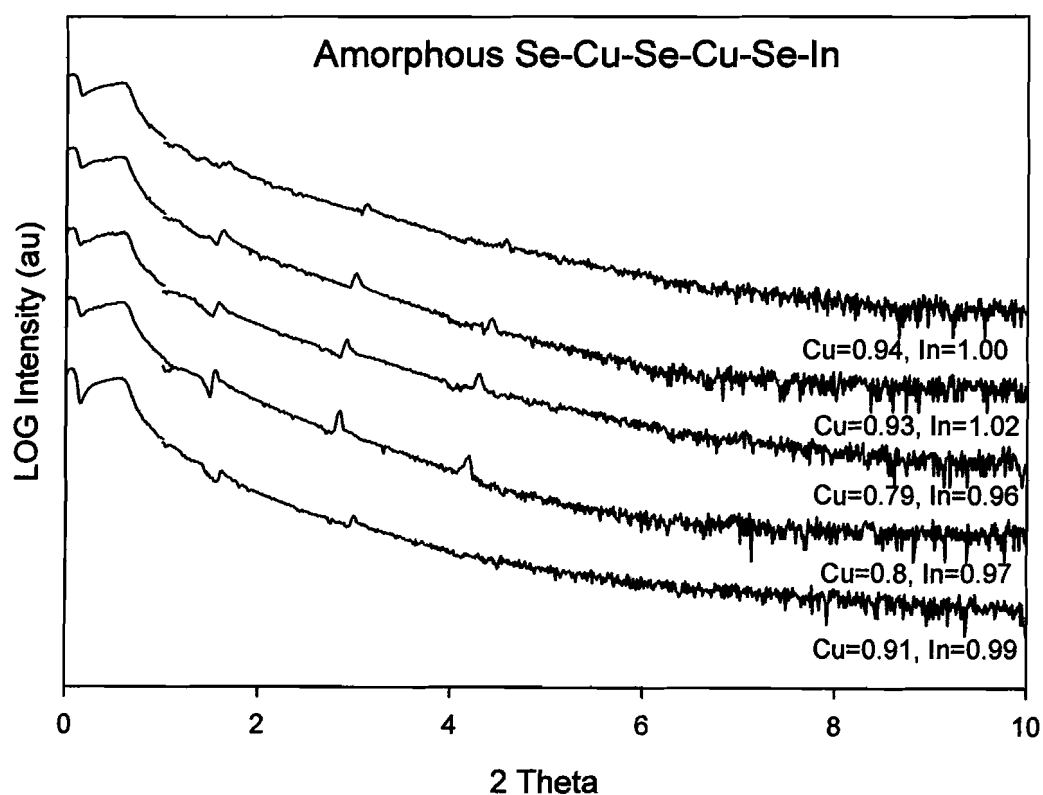


Figure 4.13. XRR patterns for some amorphous Se-Cu-Se-Cu-Se-In thin films.

A silicon supported amorphous film composed of Cu_{0.95}In_{1.02}Se₂ was annealed under nitrogen at 100 °C increments for one hour each. High angle XRD data was collected after each annealing up to 500 °C and is presented in figure 4.14.. The dominant diffraction peak in the annealed sample patterns correlates to the (112) peak of CIS. The broad peak near 29 degrees 2θ was not identified and the small sharp peak near 33 degrees 2θ is from the silicon substrate. On annealing, the CIS (112) peak becomes more intense and narrower indicating an increase in the crystallinity and crystal size of the CIS in the thin film. The 500 °C anneal plot includes an insert of the impurity peak at the same dimensional scale as the 100 °C graph. The impurity is still present after the 500 °C anneal, but has reduced in quantity and crystal size.

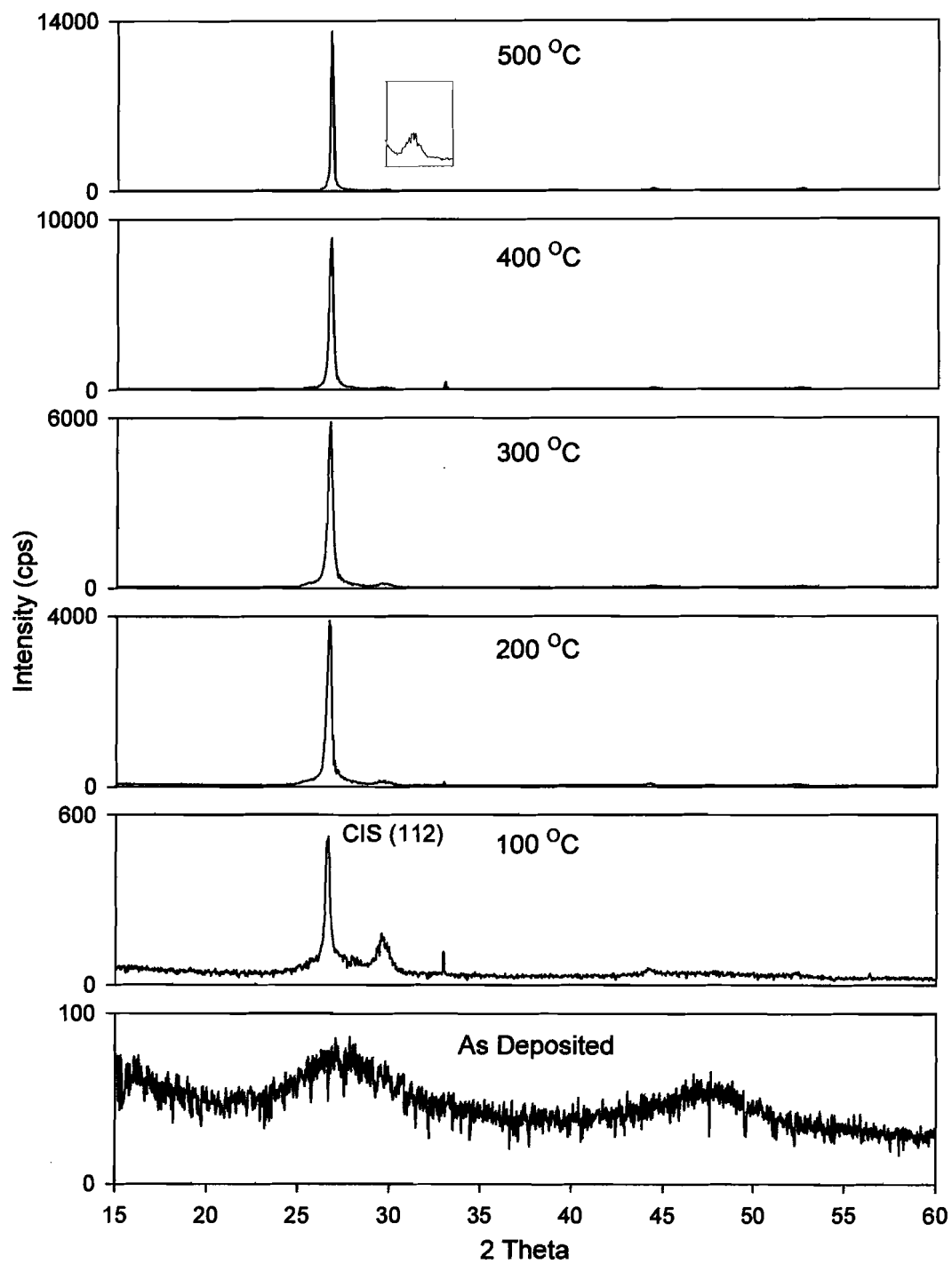


Figure 4.14. XRD patterns for an amorphous CIS film annealed in 100 °C increments to 500 °C.

The CIS crystal size was approximated using the Scherrer equation on the CIS (112) peak for the annealed samples. Figure 4.15 shows that the crystal size of the CIS increases continuously on increasing annealing temperature. The largest gain in crystal size is between 400 °C and 500 °C. This indicates that high temperature anneals are necessary, at these slow heating rates, to form large CIS crystallites.

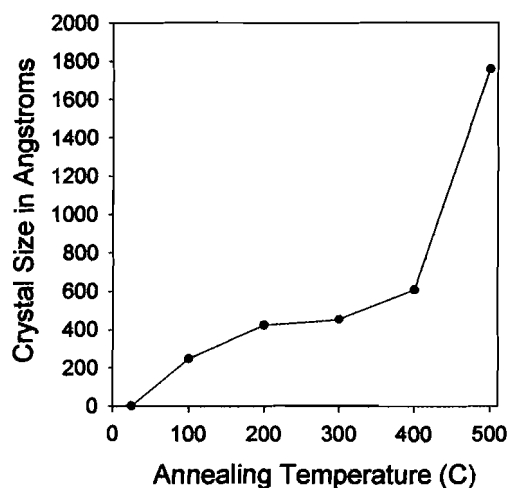


Figure 4.15. The increase in crystallite size for an amorphous CIS sample annealed at 100 °C increments to 500 °C.

Summary

Control of elemental layer repeat thickness and deposition order was used to inhibit nucleation of CIS in a thin film composed of copper, indium, and selenium. A study of the layered binary systems produced information necessary to design the precursor layer stack. The results from the copper-selenium films predicted that the 50 angstrom thick Cu-Se layers in the 60 angstrom Se-Cu-In stacks would nucleate CuSe.

This result, along with the problem with indium crystallization necessitated the use of thinner elemental layers. When the layers were thinned to a 20 angstrom repeat thickness, the elements inter-diffused and nucleated the CIS phase, similar to the co-deposited samples. To prevent the nucleation of CuSe at the Cu-Se interface, two copper layers were sandwiched between three selenium layers, reducing the Cu-Se repeat thickness. The copper and selenium now formed an amorphous mixed layer adjacent to the amorphous indium layer. The copper did not diffuse far enough through the selenium to produce the mixing of all three elements that would have resulted in nucleation of CIS. The general process of controlling a reaction pathway of a thin ternary film via elemental order and thickness by utilization of information gathered from its component binary films may be applicable to other material systems.

CHAPTER V

THE EFFECT OF SODIUM AND SUBSTITUTION OF GALLIUM ON THE NUCLEATION OF THE CHALCOPYRITE STRUCTURE

Introduction

In chapter I, I discussed how the addition of sodium to copper indium diselenide is found to have positive effects on CIS electrical properties. In chapter IV, data was presented showing how an elemental amorphous precursor stack containing copper, indium, and selenium could be deposited. In this chapter, I will discuss how the addition of sodium affects the crystallization of CIS and how the substitution of gallium for indium affects crystallization.

The Addition of Sodium

Samples with the Se:Cu:Se:Cu:Se:In layer pattern at a repeat thickness of nominally 60 angstroms were deposited with the substrate continuously exposed to a sodium flux from a thermal source. Sufficient repeat layers were deposited to form a total thickness of approximately 4800 angstroms. Microprobe was used to determine composition and XRD was performed on silicon supported samples to ascertain the presence of crystalline phases. Figure 5.1 summarizes the XRD results and compares them to similar samples containing no sodium. Numbers above or below the data points

identify the amount of sodium in the sample relative to a composition consisting of 2 seleniums. The number to the right of the data points representing samples that were crystalline on deposit indicates the as-deposited crystal size as determined by the full width at half maximum of the CIS (112) diffraction peak and the Scherrer equation.

It can be seen from the data that samples containing small amounts of sodium follow the same trends as those without sodium. Those that are Cu+In rich relative to $2(\text{Cu}+\text{In}):2\text{Se}$ are crystalline, while those with less copper and indium are generally amorphous. One sample containing a significant excess of sodium, 0.19, was crystalline with relatively small crystallites. This could be explained by a disruption of the layering by the large amount of sodium or even a substitution of the sodium for copper pushing the composition across the 1:1 Cu+In:Se composition line. In all crystalline samples containing sodium, the crystal growth has been inhibited by the presence of the sodium. From this data, it can not be conclusively determined whether the presence of the sodium inhibits or enhances CIS nucleation on deposit, however one can conclude that the creation of an amorphous CIS precursor with trace amounts of sodium is possible.

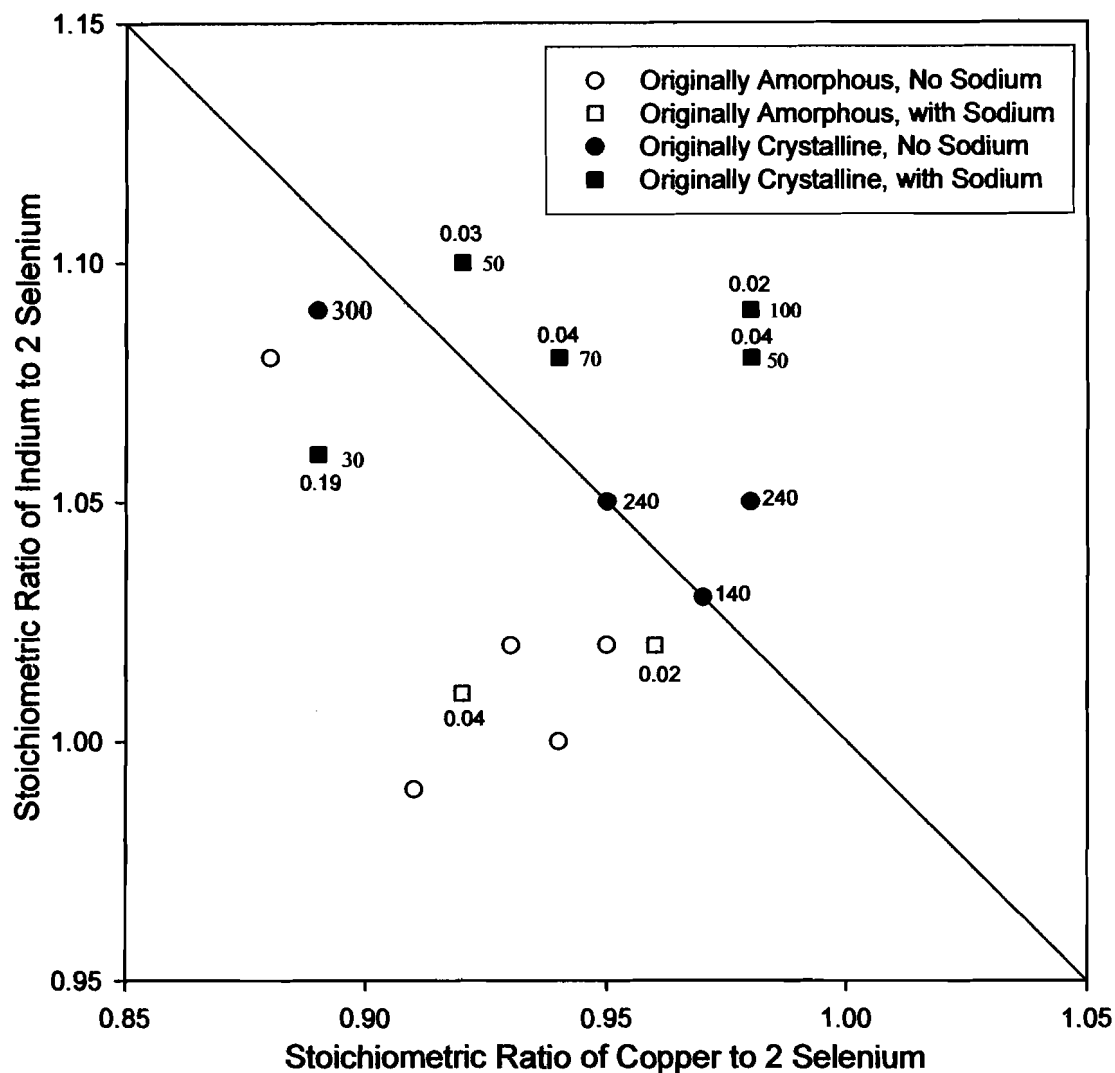


Figure 5.1. Comparison of sodium and non-sodium containing Se-Cu-Se-Cu-Se-In samples for crystallinity on deposit.

Silicon supported samples were annealed under nitrogen to a temperature of 500 °C for one hour. XRD patterns were collected on each thin film sample and crystallite size approximated using the Scherrer equation and the full width at half maximum of the CIS (112) diffraction peak. Results are summarized for both sodium and non-

sodium containing samples in figure 5.2. The data clustered between 0.9-1.0 Cu and 1.0-1.05 In tells an interesting story. All the samples that were originally amorphous grew larger crystallites than those that crystallized on deposit. Since these samples

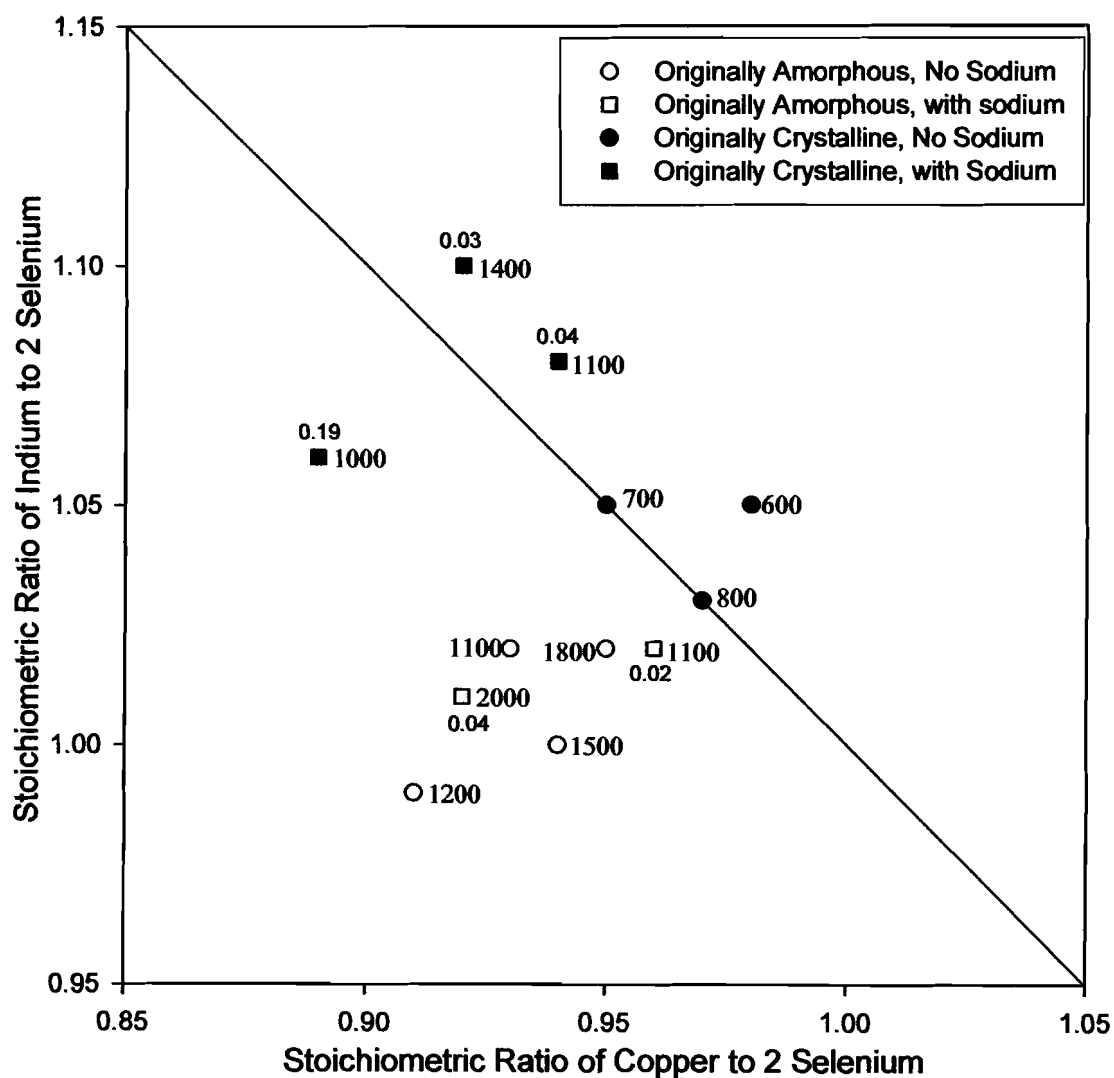


Figure 5.2. A Comparison of sodium and non-sodium containing Se-Cu-Se-Cu-Se-In samples for crystal size after annealing to 500 °C in nitrogen.

were heated at a rate of about 10 °C/min., nucleation and crystal growth was not rapid and the evolution of crystallinity in each sample occurred over time. The larger crystallite size of the originally amorphous samples is probably due to a lower nucleation density in the amorphous samples during heating leading to a higher availability of unreacted material per grain. A comparison of the crystallite size for sodium /no sodium samples is inconclusive as some produced larger and some produced smaller crystallites relative to others at similar compositions.

The Copper Gallium Diselenide Ternary System

Samples composed of selenium-gallium-copper elemental layers were deposited from thermal sources. The same copper and selenium sources used to deposit the samples described in chapter IV were used to make these samples. An effusion cell equivalent to the one used to deposit indium was used to deposit the gallium. Gallium presents a special challenge when using a quartz crystal for deposition rate monitoring. After a short period of time, the gallium on the crystal monitor begins to melt and the indicated deposition rate begins to decrease. To prevent this error, the deposition rate was determined after the gallium source had reached a stable temperature and before the drop off in rate was observed.

To determine the consistency of a Se-Ga-Cu deposition, five samples were deposited over a time span of six hours using the same deposition conditions. Each sample consisted of fifty Se-Ga-Cu repeats for a thickness of approximately 1700 angstroms for each of the five thin films. The composition of each sample was determined by microprobe with the results tabulated in Table 5.1. The results show that the deposition conditions remain stable over a six hour span.

Sample	Copper	Gallium
1	0.96	0.78
2	0.95	0.76
3	0.97	0.76
4	0.95	0.75
5	0.95	0.78

Table 5.1. Deposition consistency for five Se-Ga-Cu samples over a six hour time span.

Thicker samples of the simple Se-Ga-Cu stacking scheme were deposited at repeat thicknesses between 18 and 59 angstroms. The repeat thickness of the CGS samples was approximated using equivalent selenium and copper layer thicknesses as those of the CIS samples described in chapter IV. The XRD results for five as deposited samples are shown in figure 5.3. The CGS samples show similar trends to those of the CIS layered samples. The layered samples with excess gallium (top two) show significant CGS crystallinity as deposited. The sample with the thinner repeat thickness shows significantly more crystallinity. Like the CIS samples, all of the thicker Se-Ga-Cu layered samples have a peak near 31° , consistent with the presence of CuSe. The sample closest to being amorphous was deficient in copper and gallium.

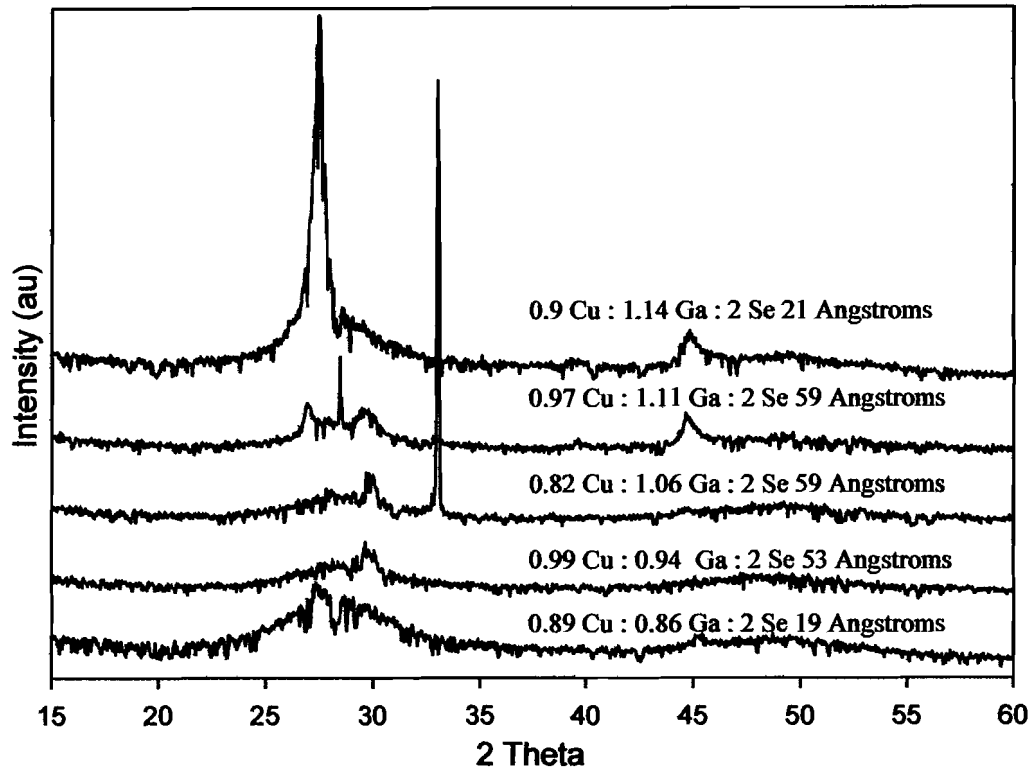


Figure 5.3. XRD patterns for as deposited Se-Ga-Cu layered films.

A Comparison of Annealed CIS and CGS Samples

Several of the samples were annealed to 500 °C for one hour each in a dry nitrogen environment. XRD was performed on the samples after annealing to identify phases and determine the crystallite size. Figure 5.4 summarizes the crystallite size data. Calculations identifying crystallite sizes greater than 2000 angstroms were rounded down to 2000 angstroms due to the limitations of the Scherrer equation. Distribution of the crystallite sizes indicates that there is no consistent difference in crystallite size for the CIS and CGS films. There is however a cluster of films

producing large crystallite sizes near $1\text{Cu}:0.95(\text{In}/\text{Ga}):2\text{Se}$. Samples closer to the stoichiometrically correct composition appear to produce the largest crystallites on annealing.

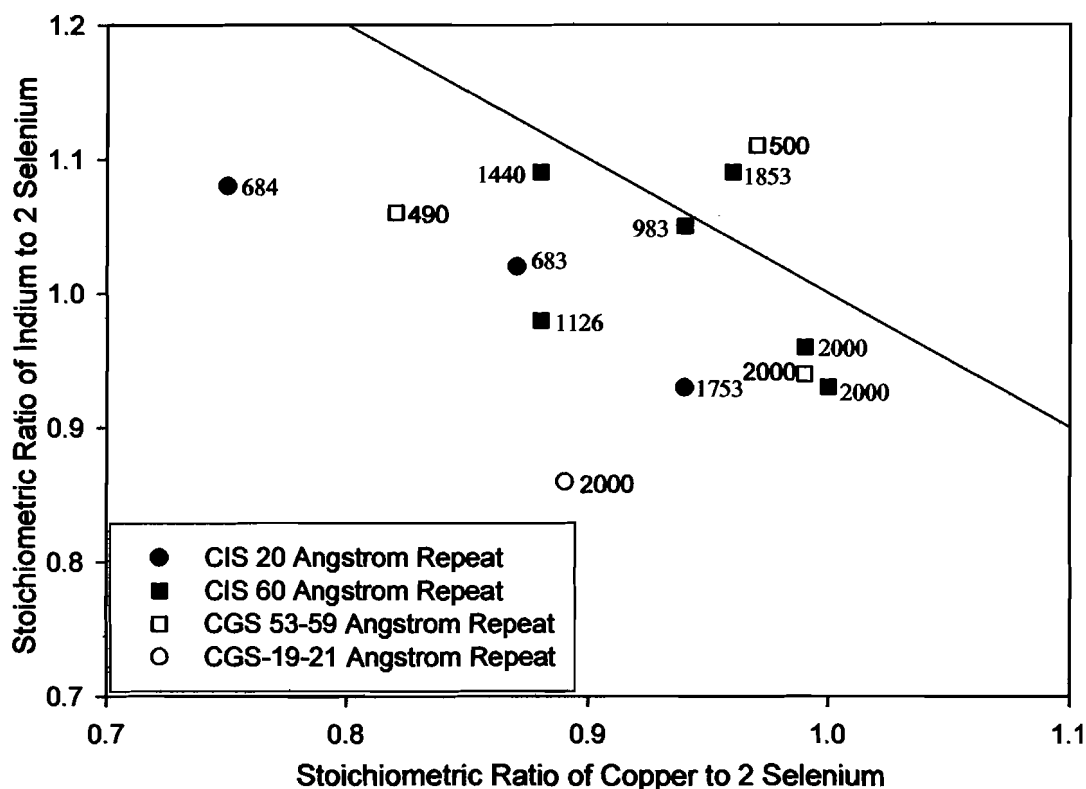


Figure 5.4. Summary of crystallite sizes for annealed films of CIS/CGS.

Summary

The presence of small amounts of sodium dispersed through the Se-Cu-Se-Cu-Se-In film does not appear to significantly affect nucleation of the CIS phase.

Additionally, there is no conclusive evidence as to how sodium affects the growth of CIS on annealing to 500 °C. Composition, specifically the Cu+In:Se ratio has the greatest effect on crystal size with as deposited amorphous films producing larger

crystallites. CGS samples with an equivalent Se-Cu-Se-Cu-Se-Ga to the amorphous CIS samples were not deposited. Samples with the simple Se-Ga-Cu layer scheme were produced and followed the trends found in the equivalent Se-In-Cu samples. It should be possible to deposit amorphous CGS and CIGS precursor films using the processes identified in chapter IV.

CHAPTER VI

SUMMARY AND CONCLUSIONS

The creation of electronic materials for devices such as solar cells, solid state displays, and other macro electronics yet to be imagined on inexpensive and flexible substrates will require the development of low temperature processes for depositing materials onto the substrate. In the case of CIGS solar cells, the high temperature deposition conditions currently used to make quality CIGS films is incompatible with the thermal limits of most flexible substrates. In addition, greater control over In/Ga diffusion will be possible using an elemental layered approach combined with moderate annealing conditions. One method of reducing thermal history is to deposit an amorphous material and use a rapid heating profile to convert the amorphous precursor directly to the crystalline phase without the creation of intermediate binary phases or small crystallites that would require extended thermal processing.

This dissertation has described the deposition and characterization of an amorphous thin film with a composition near that of CuInSe_2 (CIS). Copper-selenium and indium-selenium binary layered samples were initially investigated to identify interfacial reactions that would form undesired binary intermediate compounds resulting in the need for high temperature annealing. Although the indium-selenium did not form interfacial compounds on deposit, indium crystallized when its layer thickness exceeded 15 angstroms, disrupting the continuity of the elemental layers. Copper-

selenium elemental layers with a repeat thickness of over 30 angstroms or compositions with less than 63% selenium formed CuSe on deposit.

Several deposition schemes were investigated to identify the proper deposition pattern and thicknesses to form the CIS amorphous film. Simple co-deposition resulted in the nucleation of CIS. A simple stacking of the three elements in the order Se-In-Cu at a repeat thickness of 60 angstroms resulted in the nucleation of CuSe and sometimes CIS. The CIS most likely formed due to the disruption of the elemental layers by the growth of the CuSe. Reduction of the repeat thickness to 20 angstroms eliminated the nucleation of CuSe, as predicted by the study of the binary Cu-Se layered samples, but resulted in the nucleation of CIS, similar to the co-deposited samples.

To eliminate both the thick Cu-Se region, and prevent the intermixing of all three elements, a more complex deposition pattern was initiated. The copper and selenium repeat thicknesses were reduced into a Se-Cu-Se-Cu-Se pattern followed by deposition of the indium layer for a total repeat thickness of 60 angstroms. At a Se:Cu ratio of 2:1 and the small repeat thickness, no Cu-Se phases nucleated. Additionally, the Cu-In interface was eliminated. For this deposition scheme, films with a selenium rich composition relative to CuInSe_2 were generally amorphous. Those that were Cu-In rich always nucleated CIS on deposit. Annealing of all samples produced crystalline CIS with the as deposited amorphous samples producing significantly larger crystallites indicating a different reaction pathway from those that nucleated on deposit.

The addition of sodium during the deposition of Se-Cu-Se-Cu-Se-In samples did not significantly alter the composition range where amorphous precursors could be

deposited. Addition of sodium during the deposition process may be necessary to optimize the electrical properties of the CI(G)S layer since there will no longer be diffusion from the soda lime glass substrate as used in the modern high temperature processes. It has been predicted that the partial substitution of gallium for indium necessary to increase the band gap of the solar cell absorber layer will not prevent the deposition of amorphous CIGS precursor films. These collective results have shown that an amorphous CIGS(Na) can be produced and may lead to a low temperature route to large crystalline CIGS(Na) films.

REFERENCES

Chapter I

- (1) Noh, Myungkeun, Johnson, David C., *Angewandte Chemie, International Edition*, **1996**, 35, 2666-2669.
- (2) Harris, Fred R., Standridge, Stacey, Johnson, David C., *Journal of the American Chemical Society*, **2005**, 127, 7843-7848.
- (3) Williams, Joshua R., Johnson, Mark, Johnson, David C., *Journal of the American Chemical Society*, **2003**, 12, 10335-10341.
- (4) Villars, P., Calvert, L.D., *Pearson's Handbook of Crystallographic Data for Intermetallic Phases*, **1991**, ASM International, Materials Park, OH.
- (5) Zhang, S.B., Wei, Su-Huai, Zunger, Alex, Katayama-Yoshida, H., *Physical Review B*, **1998**, 57, 9642-9656.
- (6) Villars, P., Prince, A., Okamoto, H., *Handbook of Ternary Alloy Phase Diagrams*, **1995**, ASM International, Materials Park, OH.
- (7) Schroeder, David J., Hernandez, Jose Luis, Berry, Gene D., Rockett, Angus A., *Journal of Applied Physics*, **1998**, 83, 1519-1526.
- (8) Rockett, A., *Thin Solid Films*, **2000**, 361-362, 330-337.
- (9) Negami, Takayuki, Hashimoto, Yasuhiro, Nishiwaki, Shiro, *Solar Energy Materials & Solar Cells*, **2001**, 67, 331-335.
- (10) Kohara, Naoki, Nishiwaki, Shiro, Hashimoto, Yasuhiro, Negami, Takayuki, Wada, Takahiro, *Solar Energy Materials & Solar Cells*, **2001**, 67, 209-215.
- (11) Wada, T., Kohara, N., Nishiwaki, S., Negami, T., *Thin Solid Films*, **2001**, 387, 118-122.
- (12) Nishiwaki, Shiro, Kohara, Naoki, Negami, Takayuki, Wada, Takahiro, *Japanese Journal of Applied Physics*, 37, L71-L73.

- (13) Heske, C., Fink, R., Umbach, E., *Applied Physics Letters*, **1996**, 68, 3431-3433.
- (14) Wei, Su-Huai, Zhang, S.B., Zunger, Alex, *Journal of Applied Physics*, **1999**, 85, 7214-7218.
- (15) Lundberg, O., Lu, J., Rockett, A., Edoff, M., Stolt, L., *Journal of Physics and Chemistry of Solids*, **2003**, 64, 1499-1504.
- (16) Wei, Su-Huai, Zunger, Alex, *Journal of Applied Physics*, **1995**, 78, 3846-3856.
- (17) Wei, Su-Huai, Zhang, S.B., Zunger, Alex, *Applied Physics Letters*, **1998**, 72, 3199-3201.
- (18) Dullweber, T., Hanna, G., Rau, U., Schock, H.W., *Solar Energy Materials & Solar Cells*, **2001**, 67, 145-150.
- (19) Dullweber, Thorsten, Rau, Uwe, Contreras, Miguel A., Noufi, Rommel, Schock, Hans-Werner, *IEEE Transactions on Electron Devices*, **2000**, 47, 2249-2254.
- (20) Gabor, Andrew M., Tuttle, John R., Albin, David S., Contreras, Miguel A., Hermann, Allen M., *Applied Physics Letters*, **1994**, 65, 198-200.
- (21) Contreras, Miguel A., Egaas, Brian, Ramanathan, K., Hiltner, J., Swartzlander, A., Hasoon, F., Noufi, Rommel, *Progress in Photovoltaics: Research and Applications*, **1999**, 7, 311-316.
- (22) Dullweber, T., Hanna, G., Shams-Kolahi, W., Schwartzlander, A., Contreras, M.A., Noufi, R., Schock, H.W., *Thin Solid Films*, **2000**, 361-362, 478-481.
- (23) Knowles, A, Oumous, H., Carter, M., Hill, R., *Semiconductor Science and Technology*, **1988**, 3, 1143-1144.
- (24) Karg, F., Probst, V., Harms, H., Rimmasch, J., Riedl, W., Kotschy, J., Holz, J., Treichler, R., Eibl, O., Mitwalsky, A., Kiendl, A., *Conference Record of the IEEE Photovoltaic Specialist Conference*, **1993**, 23rd, 441-446.
- (25) Adurodija, F.O., Carter, M.J., Hill, R., *Solar Energy Materials & Solar Cells*, **1995**, 37, 203-216.
- (26) Nishiwaki, S., Satoh, T., Hashimoto, Y., Negami, T., *Journal of Materials Research*, **2001**, 16, 394-399.

Chapter III

- (1) Murray, Ritchie M.; Heyding, Robert D. *Canadian Journal of Chemistry* **1975**, 53, 878-887.
- (2) Heyding, Robert D.; Murray, Ritchie M. *Canadian Journal of Chemistry* **1976**, 54, 841-848.
- (3) Heyding, Robert D. *Canadian Journal of Chemistry* **1966**, 55, 1233-1236.
- (4) Okimura, H.; Matsumae, T.; Makabe, R. *Thin Solid Films* **1980**, 71, 53-59.
- (5) Hermann, A.M.; Fabick, L. *Journal of Crystal Growth* **1983**, 61, 658-664.
- (6) Lakshmikumar, S. T.; Rastogi, A. C. *Solar Energy Materials and Solar Cells* **1994**, 32, 7-19.
- (7) Kharchenko, M.; Boyko, B.; Panchekha, P.; Chernikov, A.; Novikov, V. *World Conference on Photovoltaic Solar Energy Conversion* **1998**, 1, 504-506.
- (8) Schimmel, M. I.; Bottechiai, O. L.; Wendt, H. *Journal of Applied Electrochemistry* **1998**, 28, 299-304.
- (9) Hergert, F.; Hock, R.; Weber, A.; Purwins, M.; Palm, J.; Probst, V. *Journal of Physics and Chemistry of Solids* **2005**, 66, 1903-1907.
- (10) Hergert, F.; Jost, S.; Hock, R.; Purwins, M. *Journal of Solid State Chemistry* **2006**, 179, 2394-2415.
- (11) Kim, S.; Kim, W.K.; Kaczynski, R.M.; Acher, R.D.; Yoon, S.; Anderson, T.J.; Crisalle, O.D.; Payzant, E.A.; Li, S.S. *Journal of Vacuum Science and Technology A* **2005**, 23, 310-315.
- (12) Kim, W.K.; Payzant, E.A.; Yoon, S.; Anderson, T.J. *Journal of Crystal Growth* **2006**, 294, 231-235.
- (13) Chraïbi, F.; Fahoume, M.; Ennaoui, A.; and Delplancke, J.L. *Condensed Matter* **2004**, 5, 88-96.

- (14) Pisarkiewicz, T.; Jankowski, H.; Schabowska-Osiowska, E.; Maksymowicz, L.J. *Opto-Electronics Review* **2003**, 11, 297-304.
- (15) Ohtani, T.; Motoki, M.; Koh, K.; Ohshima, K. *Materials Research Bulletin* **1995**, 30, 1495-1504.
- (16) Garcia, V. M.; Nair, P. K.; Nair, M. T. S. *Journal of Crystal Growth* **1999**, 203, 113-124.
- (17) Lakshmikumar, S. T.; Rastogi, A. C.; *Journal of Applied Physics* **1994**, 76, 3068-3071.
- (18) Rao, C.N.R.; Kulkarni, G.U.; Agrawal, Ved Varun; Gautam, Ujjal K.; Ghosh, Moumita; Tumkurkar, Usha *Journal of Colloid and Interface Science* **2005**, 289, 305-318.
- (19) Massalski, Thaddeus B.; Okamoto, Hiroaki; Subramanian, P.R.; Kalprzak, Linda In *Binary Alloy Phase Diagrams Second Edition*, ASM International Materials Park 1990 Volume 2 1475-1476.
- (20) Kissinger, H.E. *Analytical Chemistry* **1957**, 29, 1702-1706.
- (21) Ohtani, T.; Shohno, M. *Journal of Solid State Chemistry* **2004**, 177, 3886-3890.

Chapter IV

- (1) Noh, Myungkeun; Johnson, David C. *Angewandte Chemie, International Edition*, **1996**, 35, 2666-2669.
- (2) Harris, Fred R.; Standridge, Stacey; Johnson, David C., *Journal of the American Chemical Society*, **2005**, 127, 7843-7848.
- (3) Williams, Joshua R.; Johnson, Mark; Johnson, David C. *Journal of the American Chemical Society*, **2003**, 12, 10335-10341.
- (4) McClune, William; Clark, Harlan, et al., *Powder Diffraction File*, International Centre for Diffraction Data, 1998.